REVIEWS OF GEOPHYSICS, VOL. 26, NO. 2, PAGES 285–316, MAY 1988

Plasma Wave Observations With the Dynamics Explorer 1 Spacecraft

D. A. GURNETT

Department of Physics and Astronomy, The University of Iowa, Iowa City

U. S. INAN

STAR Laboratory, Stanford University, Stanford, California

This paper reviews the results from the plasma wave instrument on the Dynamics Explorer 1 (DE 1) spacecraft. The DE 1 spacecraft was launched on August 3, 1981, into an elliptical polar orbit with initial perigee and apogee radial distances of 1.09 and 4.65 R_E. In the roughly 6 years since the launch of the spacecraft, DE 1 has provided basic new information on a wide variety of magnetospheric plasma wave phenomena. These include auroral kilometric radiation, auroral hiss, Z mode radiation, narrow-band electromagnetic emissions associated with equatorial upper hybrid waves, whistler mode emissions, wave-particle interactions stimulated by ground VLF transmitters, equatorial ion cyclotron emissions, ion Bernstein mode emissions, and electric field turbulence along the auroral field lines. We first give a brief review of the basic plasma wave modes that can exist in the equatorial and polar regions of the magnetosphere. After the basic terminology is established, each of the above areas of plasma wave research is discussed in detail, first by reviewing the state of knowledge at the time of the DE 1 launch and then by describing the contribution made by DE 1 in the 6 years since the spacecraft was launched.

1. INTRODUCTION

This paper reviews the principal new results from the plasma wave instrument on the Dynamics Explorer 1 (DE 1) spacecraft. The study of magnetospheric plasma waves has a long and colorful history. The first report of very low frequency (VLF) radio emissions was by *Preece* [1984], who described the detection of audio frequency radio signals. These signals probably included a type of magnetospheric emission now known as chorus. Later, *Barkhausen* [1919], using a rudimentary amplifier, described observations of whistling tones that are now known as whistlers. After further investigation, *Eckersley* [1931] correctly postulated that whistlers were produced by lightning. However, the cause of the dispersion and the exact propagation path remained unknown. The first satisfactory explanation of the propagation of whistlers was provided by *Storey* [1953], who showed that low-frequency radio waves can be guided along the Earth's magnetic field lines from one hemisphere to the other in a mode of propagation now known as the whistler mode. Numerous other VLF radio phenomena were also identified by ground-based observations during the presatellite era. The best known of these is a type of emission called "dawn chorus" which was thought to be produced by charged solar particles entering the outer ionosphere during times of magnetic disturbances [*Allcock*, 1957]. The term dawn chorus was introduced by *Storey* [1953] because the signals sounded like the early morning chorus from a colony of birds. Another type of VLF radio phenomena discovered during this period was a broadband emission known as hiss which was shown to be correlated with aurorae [*Ellis*, 1957]. For a summary of these early VLF radio observations, see *Helliwell* [1965].

With the discovery of the Earth's radiation belts [*Van Allen et al.*, 1958], it soon became apparent that many of the VLF radio emissions observed on the ground during the presatellite era were associated with the trapped radiation belt particles. After more than 30 years of study it is now known that the Earth's magnetosphere contains many complex plasma wave phenomena and that these waves play an important role in controlling the distribution of plasma and energetic particles in the vicinity of the Earth. These waves include several types of electromagnetic whistler mode and ion cyclotron mode emissions, some of which account for the early ground-based VLF observations, various types of locally generated electrostatic instabilities [*Fredricks et al.*, 1968; *Kennel et al.*, 1970; *Scarf et al.*, 1970, 1971] that can be detected only by in situ spacecraft measurements, and several types of high-frequency radio emissions [*Gurnett*, 1974, 1975] that can be detected only by spacecraft located far above the ionosphere. Some of these waves play an absolutely fundamental role in the physics of the magnetosphere. In a classic work, *Kennel and Petschek* [1966] showed that electromagnetic waves driven by a loss cone instability cause pitch angle scattering of the trapped radiation belt particles, thereby regulating the equilibrium flux of the radiation belt. A thorough understanding of wave-particle interactions is now regarded as essential for understanding the physics of the radiation belts. Near the bow shock, waves driven by plasma instabilities are believed to play an important role in the heating and thermalization of nonequilibrium plasma distributions. For a review of the various types of plasma waves in the magnetosphere and their consequences, see *Shawhan* [1979].

The purpose of this paper is to describe the new plasma wave results from the Dynamics Explorer 1 spacecraft. Since the basic types of plasma waves present in the magnetosphere are now reasonably well known, the advances that have been made with DE 1 arise mainly from new capabilities of this spacecraft. Both the orbit and the instrument developments contribute to the new capabilities. The DE 1 spacecraft was launched on August 3, 1981, into an elliptical polar orbit with initial perigee and apogee radial distances of 1.09 and 4.65 R_E,

Paper number 8R0206.
8755-1209/88/008R-0206$05.00

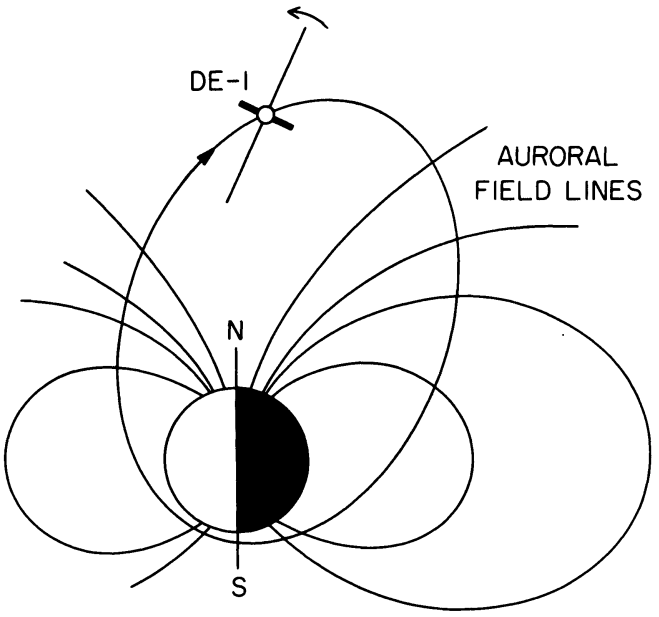

Fig. 1. The DE 1 orbit as it appeared shortly after launch. The spacecraft spin axis is perpendicular to the orbital plane. The argument of perigee advances at a rate of 108° per year, thereby providing excellent coverage of the polar cap, the auroral field lines, and the equatorial region at radial distances extending out to 4.65 R_E.

respectively. The apogee was initially located over the northern polar region, more or less as shown in Figure 1. Because the argument of perigee advances at a rate of 108° per year, in a period of a little over 3 years this orbit provides a nearly complete scan of the magnetic meridian plane from altitudes of about 600 km in the ionosphere out to radial distances of 4.65 R_E. This orbital coverage provides particularly good sampling of the auroral acceleration region and the polar cap at altitudes where relatively few data were previously available. When the apogee is located near the equator, which occurs once every 20 months, very good north-south passes are obtained through the magnetic equator. Since most previous equatorial studies involve spacecraft with orbits in or near the equatorial plane, these passes provide a unique opportunity to study the latitudinal structure of plasma and wave phenomena near the magnetic equator.

The DE 1 plasma wave instrument includes several innovative new developments. A sketch of the spacecraft showing the plasma wave antennas is shown in Figure 2, and a simplified block diagram of the plasma wave instrument is shown in Figure 3. For a detailed discussion of the instrument, see *Shawhan et al.* [1981]. Five antennas are used for performing plasma wave measurements. These include a 200-m tip-to-tip electric dipole (E_x) perpendicular to the spacecraft spin axis, a 9.0-m tip-to-tip electric dipole (E_z) parallel to the spacecraft spin axis, a 0.6-m short electric antenna (E_s), a search coil magnetometer (B_z) parallel to the spin axis, and a loop antenna (B_x) perpendicular to the spin axis. The plasma wave instrument consists of a step frequency receiver and a wideband receiver. The step frequency receiver provides measurements of the amplitudes and cross correlations of signals from any selected pair of antennas. The amplitude and correlation measurements are performed by two separate receivers referred to in Figure 3 as the high-frequency receiver and the low-frequency receiver. The high-frequency receiver provides 128 logarithmically spaced frequency channels from 100 Hz to 400 kHz, and the low-frequency receiver provides eight logarithmically spaced frequency channels from 1.78 Hz to 100 Hz. The correlator provides both in-phase and quadrature-phase (co- and quad-) correlations. These correlations can be used to measure the phase difference between the two signals. The phase provides information on several important wave characteristics. For example, if the E_x and E_z antennas are selected, the phase gives the polarization in the x-z plane, and if the E_z and B_x antennas are selected, the phase gives the Poynting flux. In addition to giving the polarization, the spin dependence of the phase between the E_x and E_z antennas can be analyzed to give two-dimensional direction-finding measurements of high-frequency electromagnetic radiation [*Calvert*, 1985].

The wideband system on DE 1 also includes a new development, which is the linear wideband receiver shown near the bottom of the block diagram in Figure 3. This receiver was designed to give a linear amplitude response over a broad dynamic range (~ 30 dB linear range with an additional 70 dB available using a digital gain selector). The wideband receiver system is used to send continuous waveforms to the ground for high-resolution spectrum processing. As will be discussed, the linear response is useful for analyzing whistler mode emissions stimulated by ground VLF transmitters.

In addition to the advances in the plasma wave instrumentation, the DE 1 plasma wave investigation also benefited greatly from several other advanced new instruments. These include the high altitude plasma instrument from Southwest Research Institute (J. Burch, principal investigator (PI)), the retarding ion mass spectrometer from Marshall Space Flight Center (R. Chappell, PI) the global auroral imager from the University of Iowa (L. Frank, PI), the energetic ion mass spectrometer from Lockheed (E. Shelley, PI), and the magnetometer from Goddard Space Flight Center (M. Sugiura, PI). The exact role of these instruments will become more apparent in the discussion that follows. For an overview of the Dynamics Explorer program, see *Hoffman and Schmerling* [1981]. For descriptions of the individual instruments, see *Burch et al.*

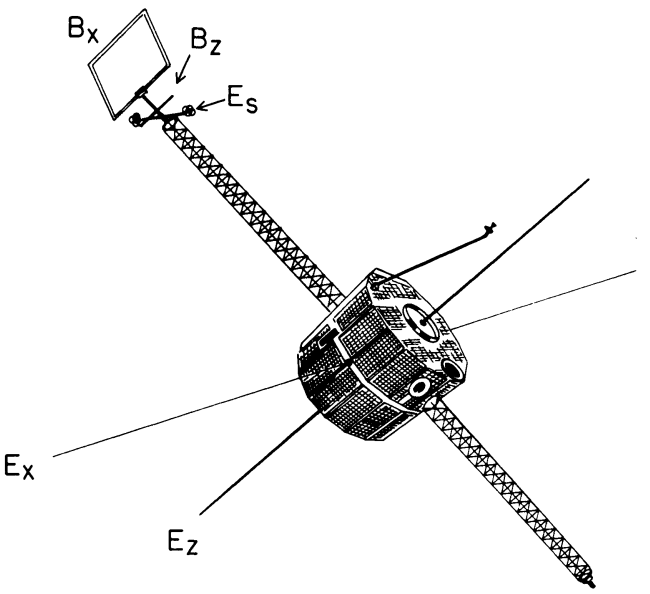

Fig. 2. A sketch of the DE 1 spacecraft showing the plasma wave antennas. The spacecraft rotates about the Z axis.

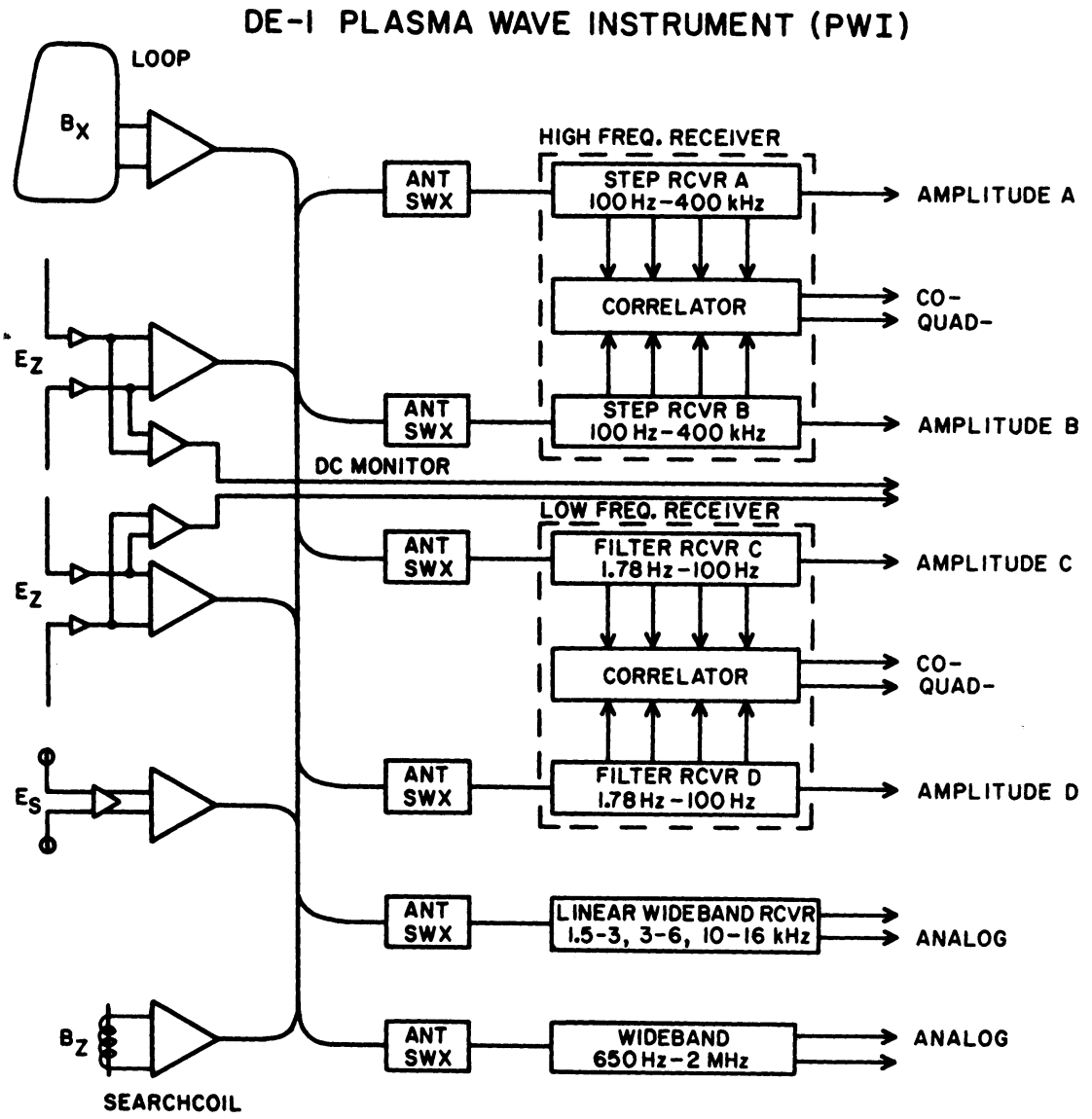

Fig. 3. A block diagram of the DE 1 plasma wave instrument. The low- and high-frequency receivers provide amplitude and correlation measurements over a frequency range from 1.78 Hz to 400 kHz. The wideband receiver provides waveform measurements in selected frequency bands extending from 10 Hz to 2 MHz.

[1981], *Chappell et al.* [1981], *Frank et al.* [1981], *Shelley et al.* [1981], and *Farthing et al.* [1981].

To organize this review we first describe the plasma wave modes that occur in the Earth's magnetosphere. The DE 1 observations are then presented in a series of sections each devoted to a specific type of plasma wave, organized more or less in order of decreasing frequency, starting with high-frequency electromagnetic emissions, such as auroral kilometric radiation, and ending with low-frequency emissions, such as auroral electrostatic noise. Where two or more waves have a close relationship, such as the electrostatic upper hybrid resonance emissions and the escaping myriametric radiation, these waves are discussed together in the same section.

2. Plasma Wave Modes

To define the terminology, it is useful to give a brief review of the types of waves that can occur in the Earth's magnetosphere. Since a complete review is beyond the scope of this article, we will concentrate mainly on the characteristic frequencies and describe how these frequencies depend on the radial distance from the Earth.

The most important characteristic frequencies of a plasma are the cyclotron frequency f_c and the plasma frequencies f_p. A cyclotron frequency and plasma frequency can be defined for each species present in the plasma. The cyclotron frequency for a charged particle of mass m_s and charge e_s is given by

$$f_{cs} = \frac{1}{2\pi} \frac{|e_s|B}{m_s} \tag{1}$$

and the plasma frequency is given by

$$f_{ps} = \frac{1}{2\pi} \sqrt{\frac{n_s e_s^2}{\varepsilon_0 m_s}} \tag{2}$$

where n_s is the number density of the sth species. Since the electron mass is much smaller than the ion mass, the electron cyclotron frequency and electron plasma frequency are much

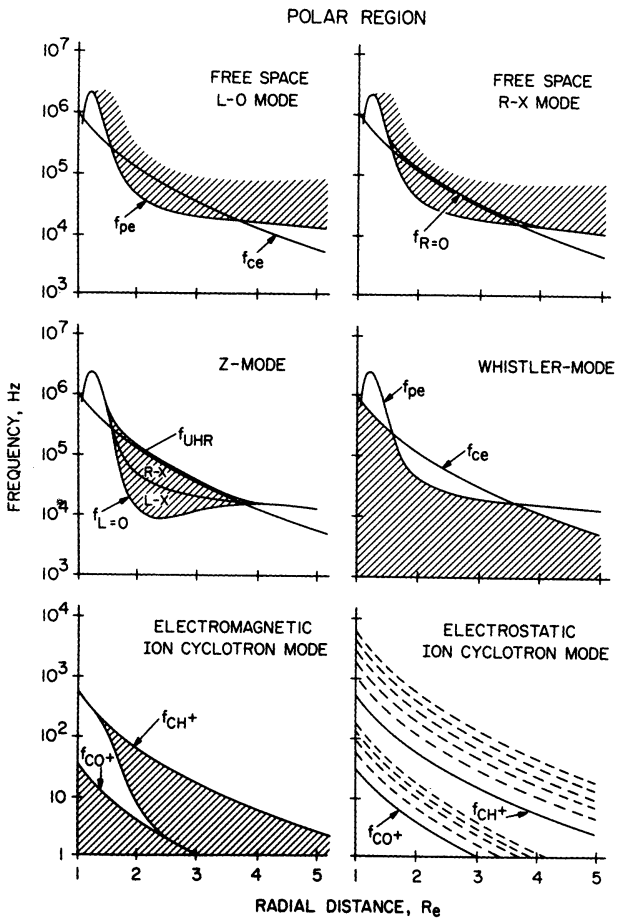

Fig. 4. The frequency range of six of the most important plasma wave modes for a representative plasma density profile over the polar region.

larger than the ion cyclotron frequency and ion plasma frequency. The high-frequency characteristics of a plasma are therefore controlled mainly by f_{ce} and f_{pe} and are relatively unaffected by the ion parameters. It is convenient to start our discussion of the various modes of propagation by first considering high frequencies, for which f_{ce} and f_{pe} are the only parameters that need to be considered. For the moment we also assume that the plasma is completely cold, so that waves associated with finite temperatures can be ignored.

As discussed in various plasma textbooks, such as those by *Stix* [1962] and *Krall and Trivelpiece* [1973], cold plasma theory predicts the existence of four separate plasma wave modes at frequencies near the electron cyclotron frequency and plasma frequency. These modes are the free-space *R-X* mode, the free-space *L-O* mode, the *Z* mode, and the whistler mode. The term free space means that the mode connects smoothly to free space ($n_e = 0$, $B = 0$). The *R* and *L* designations stand for the polarization with respect to the magnetic field (*R* for right and *L* for left), and the *X* and *O* designations stand for the type of propagation perpendicular to the magnetic field (*X* for extraordinary and *O* for ordinary). The *Z* mode is named after the so-called "*Z* trace" observed on ground ionograms [*Ratcliffe*, 1959], and the whistler mode is named after the lightning-generated signals that propagate in this mode. The low-frequency cutoffs of the *L-O* and *R-X* free-space modes are at the electron plasma frequency f_{pe} and the $R = O$ cutoff, $f_{R=O} = f_{ce}/2 + [(f_{ce}/2)^2 + f_{pe}^2]^{1/2}$. The *Z* mode is bounded by the upper hybrid resonance, $f_{UHR} = (f_{ce}^2 + f_{pe}^2)^{1/2}$, and the $L = O$ cutoff, $f_{L=O} = -f_{ce}/2 + [(f_{ce}/2)^2 + f_{pe}^2]^{1/2}$. The whistler mode propagates at frequencies below either f_{ce} or f_{pe}, whichever is lower.

The frequency ranges of the four high-frequency modes are shown in the top four panels of Figures 4 and 5 as a function of geocentric radial distance. Figure 4 is for a representative electron density profile in the polar region, and Figure 5 is for a representative electron density profile in the equatorial region. As can be seen, the frequency ranges are somewhat different in these two regions. Over the polar region the electron plasma frequency drops below the electron cyclotron frequency over a large range of radial distances, typically from about 1.5 to 4 R_E. This condition rarely, if ever, occurs in the equatorial region. One of the consequences is that the *Z* mode propagates over a relatively broad range of frequencies over the polar region but is confined to a very narrow frequency band around the electron plasma frequency in the equatorial region. Another consequence is that the low-frequency cutoff of the free-space *R-X* mode approaches very close to the electron cyclotron frequency over the polar region but is always well above the electron cyclotron frequency in the equatorial region. Also, over the polar region the upper frequency limit of the whistler mode is determined by the electron plasma frequency over a broad range of altitudes. This condition almost never occurs near the equatorial plane, where the upper fre-

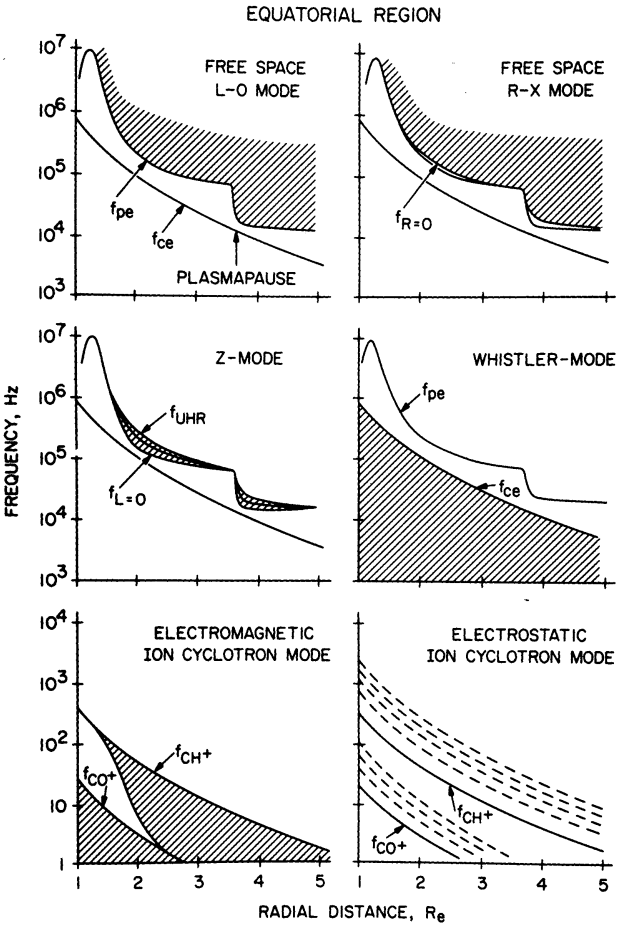

Fig. 5. The frequency range of six of the most important plasma wave modes for a representative plasma density profile near the equatorial plane. The plasma density is usually larger near the equator than over the polar region.

quency limit of the whistler mode is normally determined by the electron cyclotron frequency.

At frequencies well below the electron cyclotron frequency, ion effects start to become important. The first evidence of ion effects occurs at a frequency called the lower hybrid resonance frequency [*Stix*, 1962], which is approximately the geometric mean of the electron and ion cyclotron frequencies, $f_{LHR} \simeq (f_{ce} f_{ci})^{1/2}$. At even lower frequencies, below the ion cyclotron frequency, each species is associated with an electromagnetic mode called an ion cyclotron wave. The bottom left panels of Figures 4 and 5 show the ion cyclotron modes introduced by protons (H^+) and singly charged oxygen (O^+), which are the dominant ion species in most regions of the ionosphere and magnetosphere. Although not shown, an ion cyclotron mode branch also occurs in association with helium ions (He^+), which are usually a minor constituent.

When hot plasma effects are included, several new modes are introduced. The most important of these are the electrostatic electron cyclotron modes, which occur near half-integral, $(n + 1/2)f_{ce}$, harmonics of the electron cyclotron frequency [*Kennel et al.*, 1970], and the electrostatic ion cyclotron (EIC) modes, which occur between harmonics of the ion cyclotron frequencies [*D'Angelo and Motley*, 1962; *Kindel and Kennel*, 1971]. The approximate frequencies of the EIC modes are shown in the bottom right panels of Figures 4 and 5. Another important type of electrostatic wave, called the ion acoustic wave, occurs at frequencies below the ion plasma frequency, $f_{pi} = (m_e/m_i)^{1/2} f_{pe}$. Both the electrostatic ion cyclotron wave and the ion acoustic wave are described by an equation relation known as the Harris dispersion relation [*Harris*, 1959], modified to include the effects of ions (also see *Krall and Trivelpiece* [1973]). Hot plasma effects also occur for electromagnetic waves propagating near harmonics of the ion cyclotron frequency. The resulting modifications to the dispersion relation are sometimes referred to as the electromagnetic ion Bernstein modes [*Fredricks*, 1968]. Both the electrostatic ion cyclotron mode and the electromagnetic ion Bernstein mode usually involve waves propagating nearly perpendicularly to the static magnetic field. The interactions near harmonics of the ion cyclotron frequency are strongest when the cyclotron radii of the ions are comparable to the perpendicular wavelength of the wave.

3. AURORAL KILOMETRIC RADIATION

To order the discussion of the plasma waves detected by DE 1, we start by considering the highest frequencies. The highest-frequency plasma wave emission detected by DE 1 is auroral kilometric radiation. Auroral kilometric radiation (AKR) is an intense radio emission generated along the auroral field lines in association with discrete auroral arcs [*Gurnett*, 1974]. This radio emission usually has the highest intensities between about 100 and 400 kHz. At the time of the DE 1 launch, the polarization of the auroral kilometric radiation was an important issue. Since the radiation was known to be escaping from the Earth at frequencies well above the electron cyclotron frequency and plasma frequency, it is evident from Figure 4 that this radiation must be propagating in either the free-space *R-X* or the *L-O* mode. A measurement of the mode of propagation was important because the two modes involve quite different generation mechanisms. Theories that involved the intermediate generation of an electrostatic wave, such as the mechanisms of *Oya* [1974], *Palmadesso et al.* [1976], and *Roux and Pellat* [1979], produced radiation only in the *L-O* mode, whereas theories that involved direct generation via cyclotron resonance amplification, such as the mechanisms of *Melrose* [1973] and *Wu and Lee* [1979], produced radiation primarily in the *R-X* mode.

Two determinations of the mode of propagation of auroral kilometric radiation had been made prior to the DE 1 observations, one by *Gurnett and Green* [1978] and the other by *Kaiser et al.* [1978]. Both concluded that the radiation was generated in the *R-X* mode. *Gurnett and Green* [1978] based their conclusion on a low-frequency cutoff observed near the electron cyclotron frequency which was interpreted as the $R = O$ cutoff (see Figure 4), and *Kaiser et al.* [1978] based their conclusion on direct polarization measurements by Voyager 1 and 2. Although both results were consistent, doubts persisted, in the first case because the low-frequency cutoff cannot rule out the possibility of an *L-O* mode, and in the second case because the Voyager 1 and 2 measurements were made near the equatorial plane, where the direction of propagation makes a large angle (nearly perpendicular) to the magnetic field in the source. Since the polarization is defined with respect to the magnetic field in the source region, polarization measurements should be made under conditions when the propagation direction is nearly parallel to the magnetic field.

Since DE 1 passes directly over the auroral regions on every orbit, the DE 1 orbit provided a nearly ideal geometry for measuring the polarization of the auroral kilometric radiation. The first DE 1 polarization measurements were reported by *Shawhan and Gurnett* [1982]. These measurements showed that the dominant polarization was right-handed with respect to the magnetic field, thereby confirming the earlier conclusions that the radiation is generated primarily in the *R-X* mode. A frequency-time spectrogram of an auroral kilometric radiation event for which polarization measurements were obtained is shown in Figure 6. The auroral kilometric radiation consists of the intense emissions above the electron cyclotron frequency from about 1620 to 1710 UT. The step frequency correlator measurements for a single 32-s sweep around 1648 UT are shown in Figure 7. The crucial parameter for determining the polarization is the phase θ between the E_x and E_z signals. As the frequency sweep passes through the frequency range from about 100 to 400 kHz, the phase develops a clearly defined square wave pattern, switching back and forth between 90° and 270°. This square wave pattern is caused by the spacecraft rotation. Times when the E_x antenna axis is aligned along the nadir (local vertical) are indicated by the vertical dashed lines. In the southern hemisphere, where these measurements were obtained, the observed pattern, $\sim 90°$ just after the nadir crossing, switching to $\sim 270°$ one-half spin later, is indicative of a right-hand polarization wave. The majority of the intense kilometric radiation events are similar to the case shown in Figures 6 and 7.

Although the most intense kilometric radiation is usually right-hand polarized, left-hand-polarized emissions also occur. In a study of a large number of events, *Mellott et al.* [1984] clearly showed that a weak left-hand-polarized *L-O* component is also present. On a given pass over the auroral zone it is usually found that either the right-hand-polarized *R-X* mode radiation occurs by itself or both the *R-X* mode and the *L-O* mode are present simultaneously. When the *L-O* mode emission is present, the frequency of this emission is usually below the frequency of the *R-X* mode. This relationship is illustrated

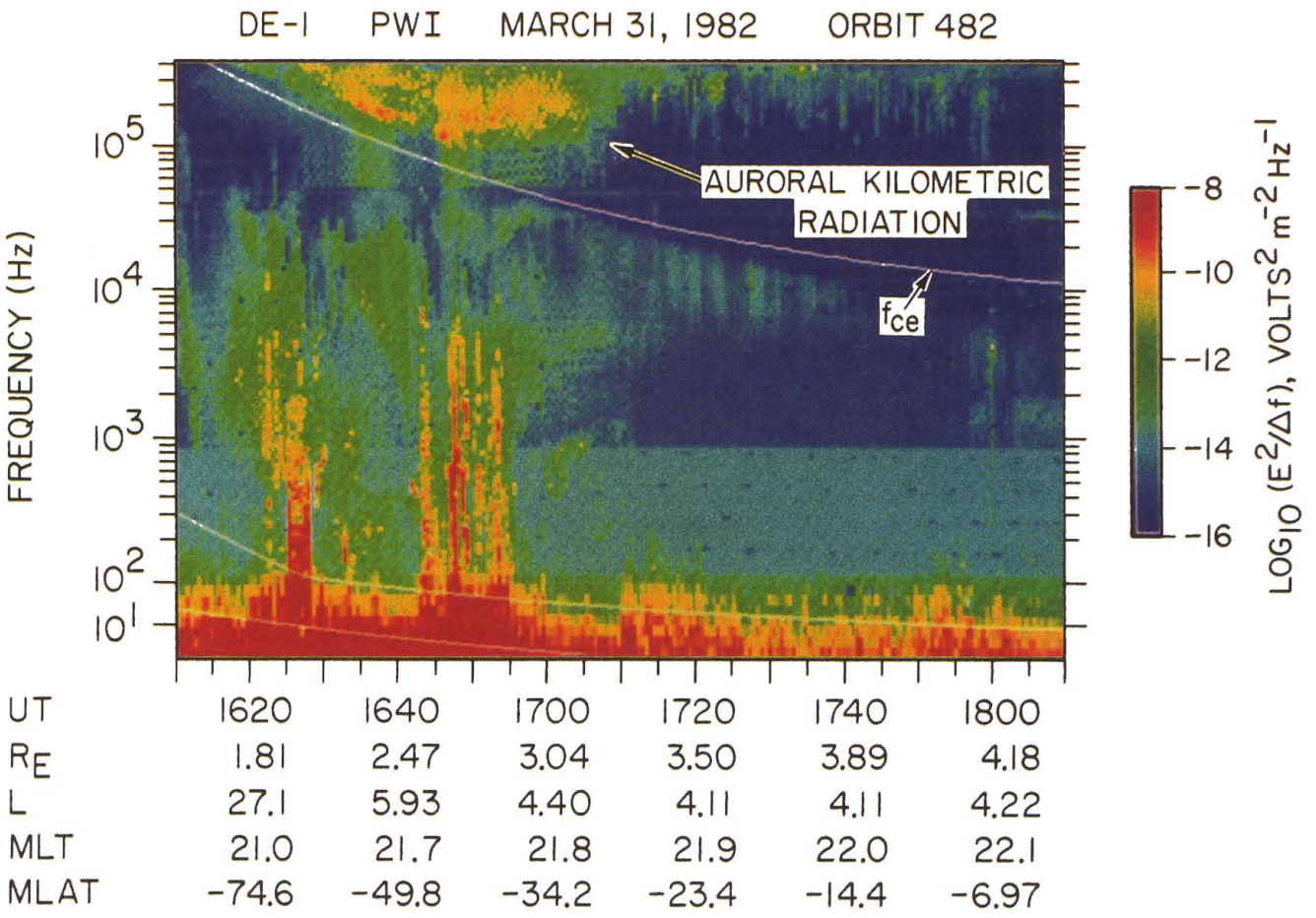

Fig. 6. A typical DE 1 electric field spectrogram obtained during a high-altitude pass over the auroral zone. The intense broadband radio emission evident at frequencies above the electron cyclotron frequency is auroral kilometric radiation.

in Figure 8, which shows a polarization spectrogram during a nighttime pass over the auroral zone. Red indicates right-hand polarization and green indicates left-hand polarization. *Mellott et al.* [1984] interpret this frequency difference as indicating that the *L-O* mode radiation is emitted at larger wave normal angles than is the *R-X* mode radiation. This difference in the radiation pattern allows the *L-O* mode radiation to be observed at a greater distance and at a lower frequency than for the *R-X* mode radiation.

Several factors suggest that the *L-O* mode radiation may simply be a by-product of the *R-X* mode generation. When both components are present, *Mellott et al.* [1984] found that the amplitudes of the two components are closely correlated, with the *O* mode about a factor of 50 less intense than the *X* mode. Also, even though the *O* mode can propagate at frequencies well below the electron cyclotron frequency (see Figure 4), the *O* mode radiation never extends below the electron cyclotron frequency, suggesting that both emissions are produced at the same frequency. Furthermore, recent studies of the fine structure by *Benson et al.* [1988] show that both components have essentially identical spectral characteristics. These facts are all consistent with a weak (2%) conversion of the *R-X* mode radiation to *L-O* mode radiation in the source region, possibly due to scattering by density irregularities or some other relatively inefficient mode conversion process. *L-O* mode radiation can also be produced by direct cyclotron resonance amplification [*Melrose et al.*, 1984]. However, it is difficult to account for all of the observed characteristics if the *L-O* mode radiation is generated independently of the *R-X* mode radiation.

The presence of harmonic structure in the auroral kilometric radiation spectrum has also been studied with the DE 1

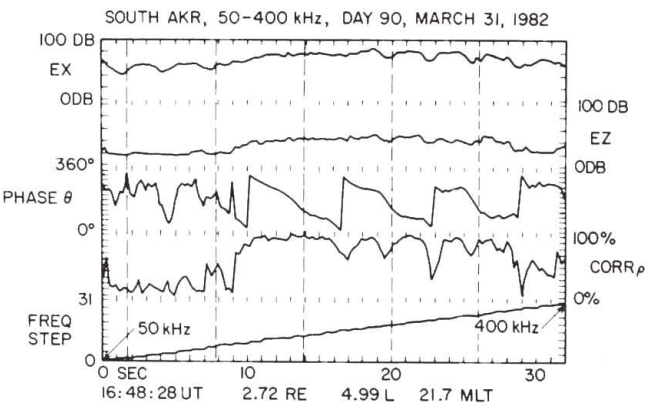

Fig. 7. An expanded plot showing one sweep of the high-frequency receiver starting at 1648:28 UT from Figure 6. The phase θ is the relative phase angle between the E_x and E_z antennas. The square wave modulation of θ, between 90° and 270° near the end of the plot, is caused by the spacecraft rotation. The observed pattern is indicative of a right-hand-polarized wave (*R-X* mode) [from *Shawhan and Gurnett*, 1982].

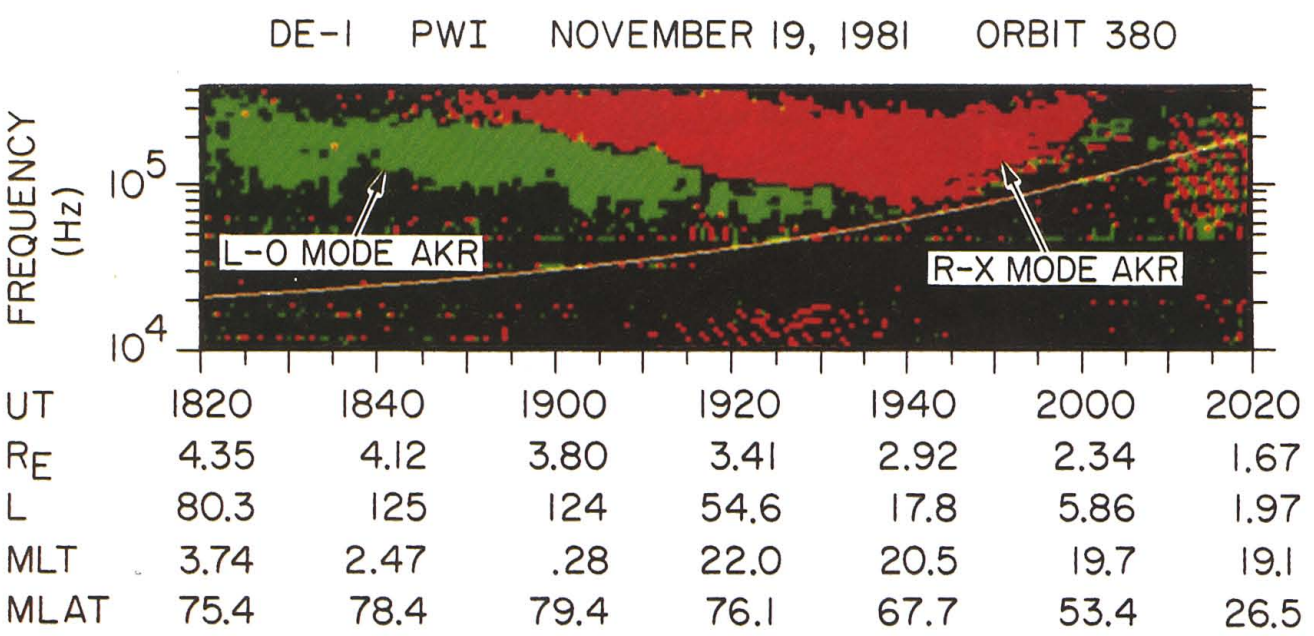

Fig. 8. A polarization spectrogram showing right-hand (red) and left-hand (green) polarized auroral kilometric radiation. The strongest AKR is usually right-hand polarized. However, left-hand-polarized AKR also occurs. When it does occur, the left-hand component occurs at frequencies below those of the right-hand component [from *Mellott et al.*, 1984].

plasma wave instrument [*Mellott et al.*, 1986]. The existence of emission near the second harmonic (twice the fundamental emission frequency) was first observed in ISIS 1 data by *Benson and Calvert* [1979], who tentatively ascribed it to nonlinearities in the instrument response. However, several mechanisms were proposed for generating second-harmonic radiation [*Lee et al.*, 1980; *Wu and Qiu*, 1983; *Melrose et al.*, 1984], and later studies by *Benson* [1982, 1984, 1985] produced evidence that the ISIS 1 harmonic emissions were of natural origin. Still, the origin of the signals remained controversial [*Calvert*, 1983; *Benson*, 1985]. The difficulty was that the ISIS 1 observations were obtained near the source, where the fundamental emission is very intense, thereby saturating the receiver and making it difficult to distinguish instrument effects from true harmonic emissions. Because DE 1 passes over the auroral zone at much higher altitudes than does ISIS 1, the intensities are lower, and instrument distortion effects are less likely. Also, as will be discussed below, the polarization measurement capability of DE 1 provided further strong evidence that the harmonic effects are not instrumental.

An example of a DE 1 observation of harmonic structure in the auroral kilometric radiation is shown in Figure 9 [from *Mellott et al.*, 1986]. The top panel shows the electric field intensity spectrogram from the E_x antenna, and the bottom panel shows the polarization, with red indicating right-hand and green indicating left-hand. The fundamental and harmonic components of the kilometric radiation are clearly evident in the intensity spectrogram. As can be seen, the fundamental is left-hand polarized (green), and the harmonic is right-hand polarized (red). This reversal of the polarization provides strong evidence that the second-harmonic component is of natural origin. No instrumental effect is known that can produce a polarization reversal of the harmonic component. Unfortunately, events of the type shown in Figure 9 are quite rare. Only a few percent of the auroral zone passes show clearly resolved fundamental and second-harmonic emissions. It is possible that harmonic emissions occur a large fraction of the time but are obscured by the fundamental emission, which is more intense and extends over a broader bandwidth, typically more than a factor of 2 in frequency.

Because the auroral kilometric radiation was known to be associated with the aurora [*Gurnett*, 1974] the inclusion of an auroral imager on DE 1 provided an ideal opportunity to further investigate this association. The first results of a comparison of the DE 1 auroral images and auroral kilometric radiation spectrums are presented by *Huff et al.* [1988]. These comparisons confirmed the association reported by *Gurnett* [1974] and provide dramatic new evidence that the radiation is generated near the electron cyclotron frequency.

If the auroral kilometric radiation is generated at the electron cyclotron frequency, a unique source position can be determined from the intersection of the electron cyclotron frequency surface and a line along the direction of arrival. The geometry involved is illustrated in Figure 10. The direction of arrival can be obtained using the two-dimensional direction-finding capability of DE 1. Once the source position has been determined, the source can be compared with the aurora by tracing a magnetic field line from the source to the point where the auroral optical emissions occur, which is assumed to be at an altitude of 200 km. When such comparisons were made, the results were very striking. A typical example of an auroral image obtained during an intense auroral kilometric radiation event is shown in Figure 11. Points 1, 2, 3 and 4 are the source positions inferred from direction-finding measurements at frequencies of 104, 136, 170, and 218 kHz. Point 4 is closer to the Earth than is point 1 because the cyclotron frequency surface is closer to the Earth at 218 kHz than at 104 kHz. The dashed lines are the magnetic field lines from these source positions traced down to the 200-km level. As can be seen, the magnetic field lines terminate almost exactly on a bright auroral feature.

Many comparisons of the type shown in Figure 11 have been performed, mostly with auroral images that show well-defined bright features. In virtually all cases the magnetic field line through the source coincides almost exactly with the bright auroral feature. When the auroral feature moves, such

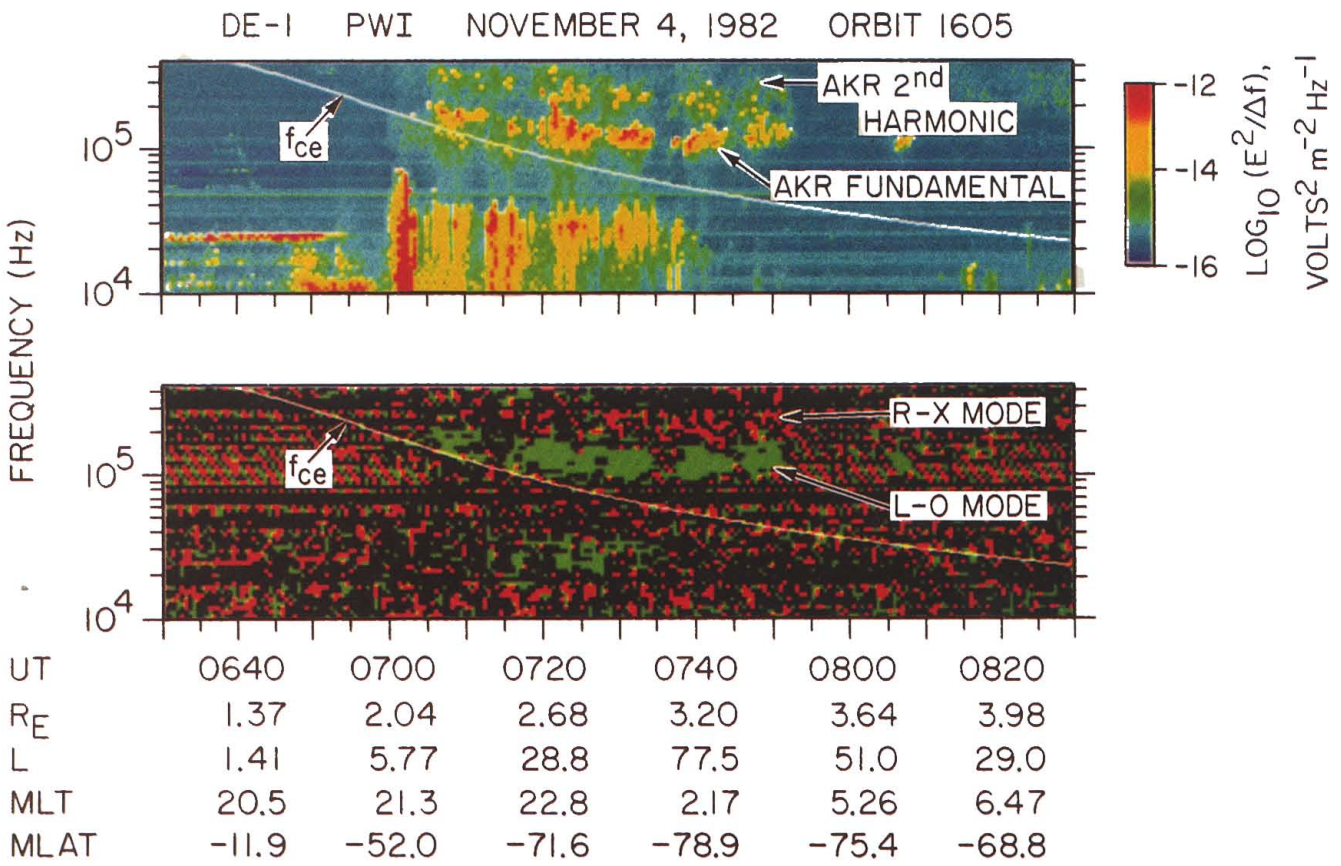

Fig. 9. A spectrogram showing fundamental and second-harmonic AKR. In this case the fundamental is left-hand polarized (*L-O* mode), and the harmonic is right-hand polarized (*R-X* mode). The polarization reversal provides strong evidence that the harmonic is not produced by distortion in the instrument [from *Mellott et al.*, 1986].

as during an auroral substorm, the kilometric radiation source moves accordingly. This correspondence holds for a wide variety of viewing geometries, including sources located on the east and west sides of the Earth as well as near the meridian through the spacecraft. In addition to providing strong evidence that the radiation is generated very close to the electron cyclotron frequency, these observations also show that the radiation is emitted over a broad range of wave normal angles. Since many of the current theories of auroral kilometric radiation [*Melrose*, 1976; *Wu and Lee*, 1979] predict maximum growth rates over a relatively narrow range of wave normal angles nearly perpendicular to the magnetic field, these observations suggest that considerable scattering occurs in the vicinity of the source.

4. Auroral Hiss and Z Mode Radiation

Auroral hiss and *Z* mode radiation occur over the auroral zone and polar cap at frequencies below the auroral kilometric radiation. Because these two types of emissions tend to occur in the same frequency range, and have similar characteristics, they will be discussed together. Auroral hiss is a whistler mode emission produced by auroral electron beams, and *Z* mode radiation is a broadband emission observed over the auroral zone and polar cap. Although auroral hiss has been extensively studied over the past 20 years [*Gurnett*, 1966; *Jorgensen*, 1968; *Gurnett and Frank*, 1972; *Laaspere and Hoffman*, 1976], only a few observations of high-latitude *Z* mode radi-

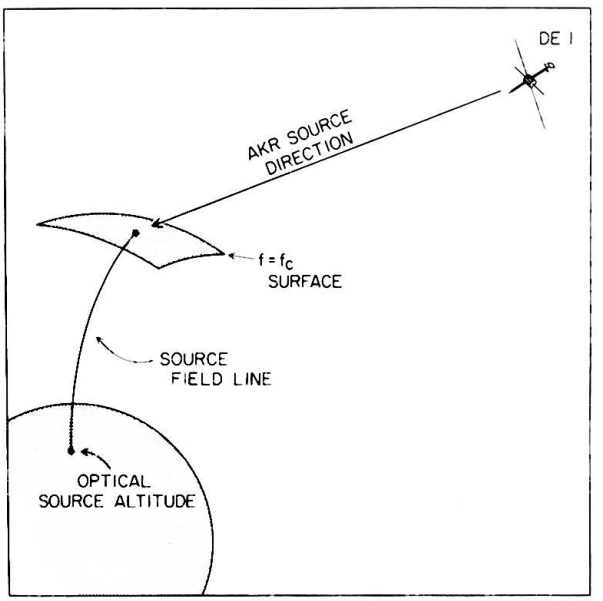

Fig. 10. The geometry used by DE 1 to determine the source position of the auroral kilometric radiation (see Figure 11). The AKR source direction is determined from the phase and amplitudes of the electric fields detected by the E_x and E_z antennas. The source position is determined by the intersection of the arrival direction with the $f = f_{ce}$ surface, assuming that the radiation is generated near the electron cyclotron frequency.

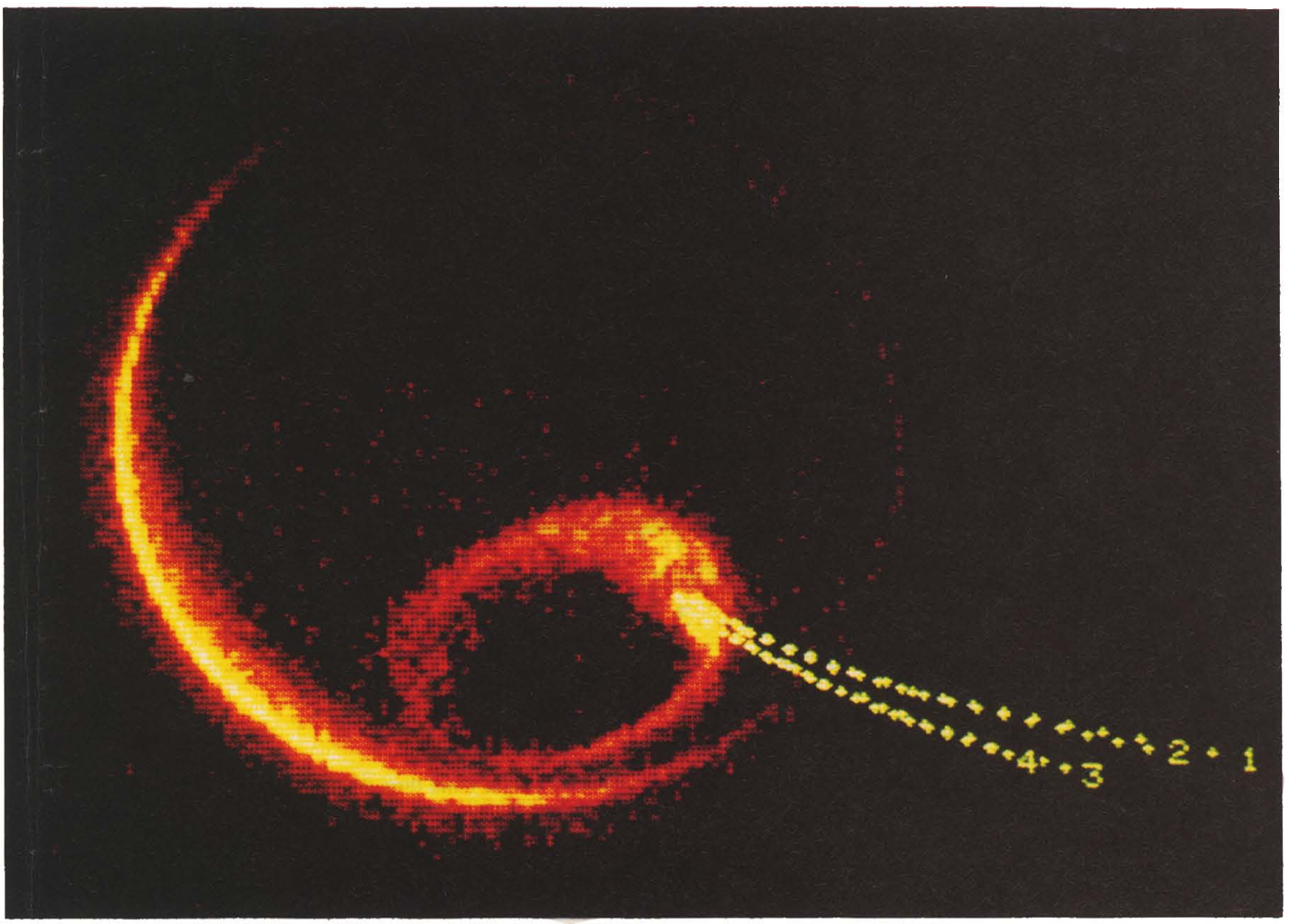

PWI

AKR SOURCE #	UT	WAVE FREQUENCY
1	0445	104 kHz
2	0445	136 kHz
3	0445	170 kHz
4	0445	218 kHz

Fig. 11. Comparisons of an auroral image taken by the DE 1 auroral imager [*Frank et al.*, 1981] and AKR source positions determined using the techniques shown in Figure 10. The dashed lines show the magnetic field lines through the AKR source. These field lines intersect bright features in the auroral image [from *Huff et al.*, 1988].

ation have been reported [*Gregory*, 1969; *Hartz*, 1969; *Muldrew*, 1970; *Calvert*, 1981], mostly at low altitudes over the polar regions. An example of a DE 1 spectrogram with auroral hiss and Z mode radiation is shown in Figure 12. This pass starts at high altitudes over the polar cap and crosses over the auroral zone at about 0630 UT. The auroral hiss consists of the funnel-shaped feature extending from 0520 to 0650 UT, and the Z mode radiation consists of the weak emission extending downward from the electron cyclotron frequency. The auroral hiss has a sharp upper cutoff at a frequency which has been identified by *Gurnett et al.* [1983] as the electron plasma frequency. As was shown in Figure 4, when the plasma frequency is below the electron cyclotron frequency, the upper frequency limit of the whistler mode is at the electron plasma frequency. As the wave frequency approaches the electron plasma frequency, the resonance cone of the whistler mode

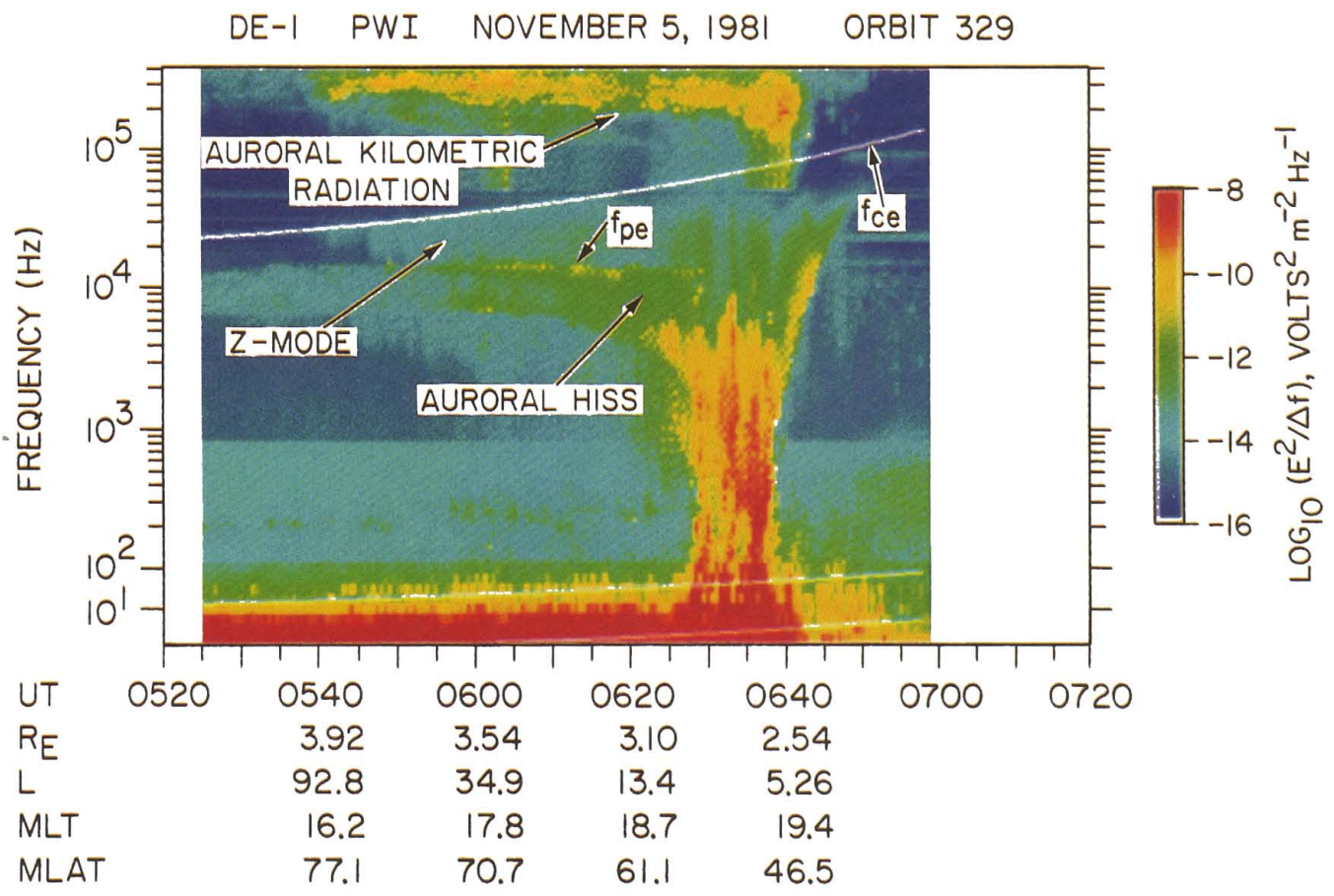

Fig. 12. A spectrogram for a high-altitude DE 1 pass over the auroral zone in which three types of auroral plasma wave emissions can be seen: auroral kilometric radiation, Z mode radiation, and auroral hiss.

shrinks to zero ($\theta = 0°$). For the upper cutoff of the auroral hiss to be at the electron plasma frequency the auroral hiss must be refracted to near-parallel propagation ($\theta = 0°$) as the wave frequency approaches the plasma frequency. Studies of the wave normal direction near the upper cutoff by *Gurnett and Persoon* [1987] show that near the upper cutoff the parallel propagation condition is usually satisfied to a good approximation so that the cutoff can be used to determine the plasma frequency. The electron density can then be computed from the cutoff using equation (2).

Two studies of the electron density have been completed using the upper cutoff of the auroral hiss. The first study, by *Persoon et al.* [1983], concentrated on measurements of the electron density over the polar cap and provided the first determination of the radial profile of the electron density over the polar cap at radial distances above 2 R_E. This profile is shown in Figure 13. The electron density varies systematically with radial distance, decreasing from about 30 cm^{-3} at 2 R_E to about 1 cm^{-3} at 4.6 R_E. Large variations, by up to a factor of 10, occur from pass to pass. The second study, by *Persoon et al.* [1988] concentrated on electron density measurements in the auroral zone and confirmed the existence of a plasma cavity along the auroral field lines at radial distances from 2 to 4 R_E, as first reported by *Calvert* [1981]. A typical electron density plot for a pass through the auroral plasma cavity is shown in Figure 14. Typically, the electron density decreases by a factor ranging from 2 to 10 as the spacecraft crosses the

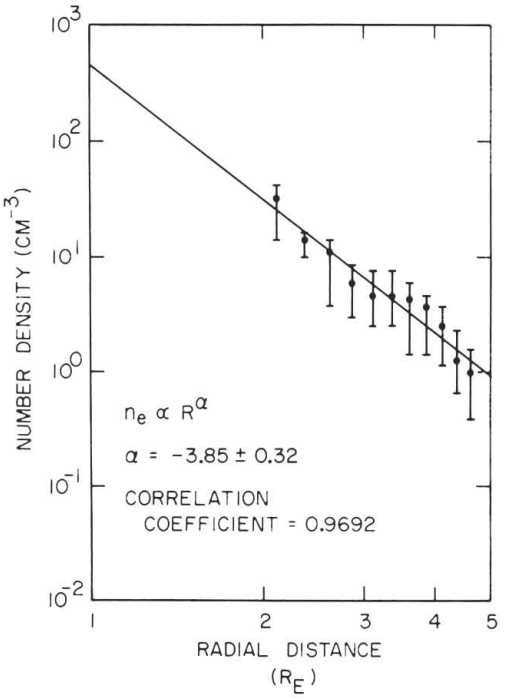

Fig. 13. The electron density at high altitudes over the polar region obtained from the upper cutoff of auroral hiss.

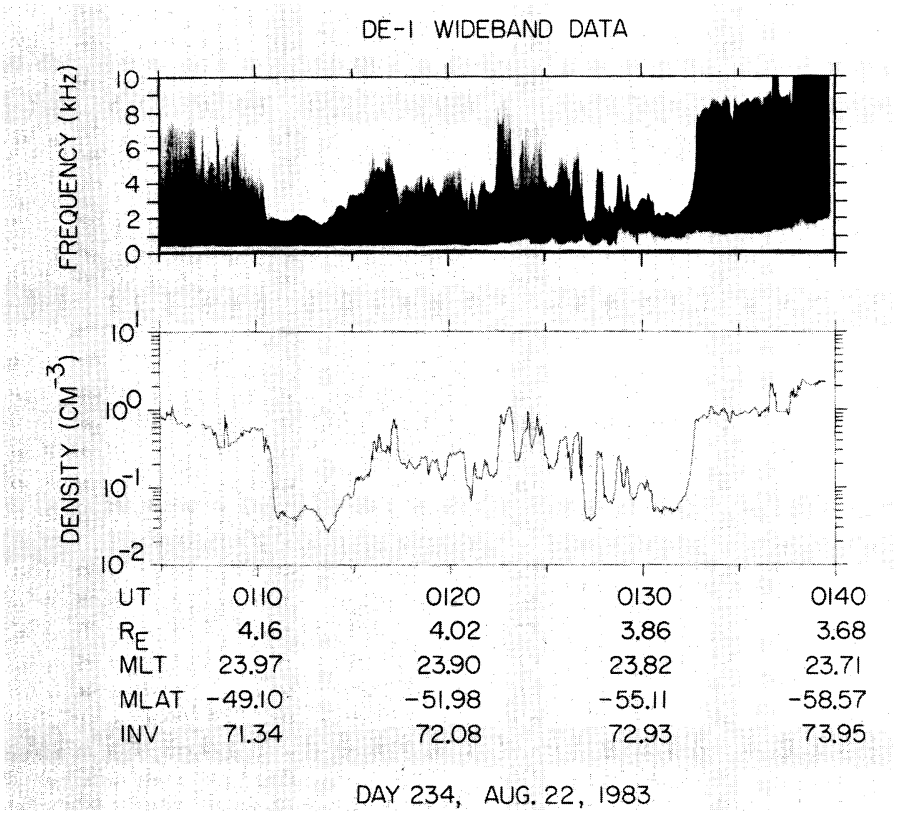

Fig. 14. An example of a DE 1 pass through the auroral plasma cavity. The plasma cavity is characterized by a strongly depleted electron density. This depletion can be seen in the upper cutoff of auroral hiss, which is at the local plasma frequency. The bottom panel shows the electron density obtained from the auroral hiss cutoff.

auroral L shells at radial distances of 2–4 R_E. In the cavity the electron density is often highly structured, with variations of up to a factor of 2 on spatial scales as small as a few kilometers. Low-energy ions are also observed streaming upward along the magnetic field lines within the cavity. This ion outflow is sufficient to deplete the plasma density within the cavity on time scales of a few hours.

Because the frequency range of the Z mode overlaps the whistler mode (see Figure 4), it is often difficult to distinguish auroral hiss from Z mode radiation. The extent of this overlap is illustrated in Figure 15, which shows a spectrum from 0542 to 0544 UT for the event in Figure 12. In this case the two emissions can be distinguished because the auroral hiss is more intense, which causes an abrupt drop in the intensity at the electron plasma frequency. If the two emissions have comparable intensities, or if the upper cutoff of the auroral hiss is not sharp, the two modes are very difficult to distinguish. This ambiguity is present after about 0624 in Figure 12.

The funnel-shaped frequency-time characteristic of the auroral hiss is a propagation effect which occurs for whistler mode waves with wave vectors near the resonance cone. For many years it has been known that auroral hiss is propagating at wave normal angles near the resonance cone, in a region where the whistler mode is quasi-electrostatic [*Smith*, 1969; *Mosier and Gurnett*, 1969; *Gurnett and Frank*, 1972; *James*, 1976]. For wave normal angles near the resonance cone, the ray path is perpendicular to the resonance cone and propagates at an angle ψ_{res} relative to the magnetic field, as shown in Figure 16. The angle ψ_{res} is given by

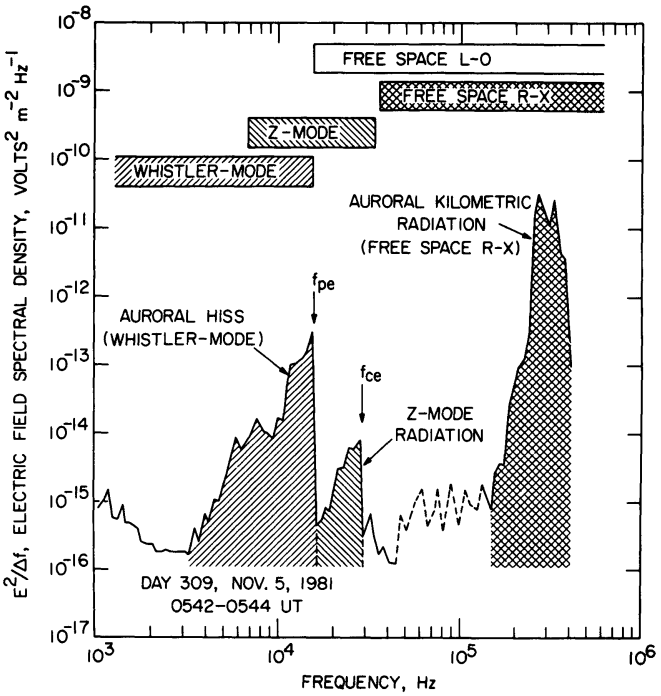

Fig. 15. Typical electric field spectrums of auroral kilometric radiation, Z mode radiation, and auroral hiss. Because the frequency range of the Z mode and the whistler mode overlap, it is sometimes difficult to distinguish auroral hiss from Z mode radiation. In this case the two types of noise can be distinguished because of the abrupt cutoff of the auroral hiss at the electron plasma frequency.

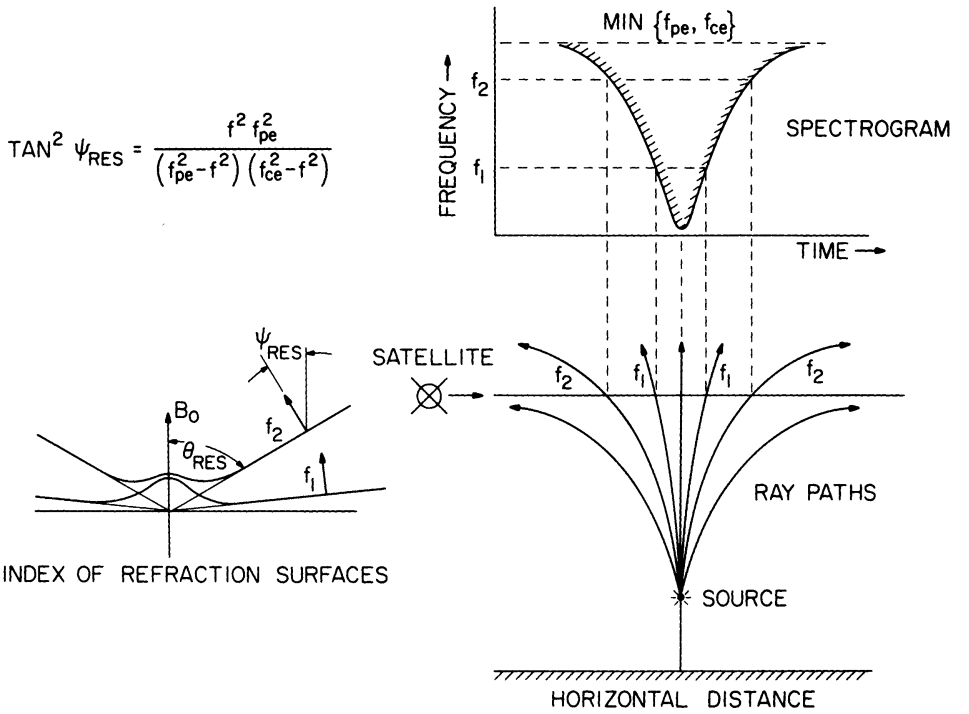

Fig. 16. An explanation of the funnel-shaped frequency-time spectrum of auroral hiss. For whistler mode waves propagating near the resonance cone, the angle ψ_{res} between the ray path and the magnetic field increases with increasing frequency. Therefore a satellite approaching a source detects the highest frequencies first, thereby producing the funnel-shaped frequency-time spectrum.

$$\tan^2 \psi_{res} = -\frac{S}{P} \simeq \frac{f^2 {f_{pe}}^2}{({f_{pe}}^2 - f)({f_{ce}}^2 - f^2)} \quad (3)$$

where S and P are defined by *Stix* [1962], and the approximation is valid whenever S is much greater than 1 (high-density approximation). Equation (3) shows that at low frequencies the ray path is almost parallel to the magnetic field. As the frequency increases, the angle ψ_{res} increases, approaching 90° as the wave frequency approaches either f_{pe} or f_{ce}, whichever is smaller. For a wave propagating upward, toward a region of decreasing f_{pe} and f_{ce}, the ray path deviates more and more from the magnetic field, eventually propagating horizontally as f approaches min (f_{pe}, f_{ce}). The resulting ray paths are illustrated in Figure 16. For a satellite passing horizontally over the source, the highest frequencies are detected first, with lower and lower frequencies occurring as the satellite approaches the field line through the source. The result is the funnel-shaped frequency-time dependence. Although V-shaped features have been previously observed in auroral hiss spectrums [*Gurnett and Frank*, 1972], the DE 1 observations provided the first evidence of "flaring" of the funnel as the frequency approaches the upper cutoff at min (f_{pe}, f_{ce}). Ray path computations by *Gurnett et al.* [1983] show good fits for source positions located at altitudes of about 0.7–0.9 R_E. Poynting flux observations also confirm that the emissions are propagating upward, in agreement with the above picture. Downward propagating auroral hiss emissions also occur [*Gurnett and Frank*, 1972]. The downward propagating auroral hiss emissions are observed mainly at low altitudes, below ~ 1 R_E. It seems likely that the funnel-shaped auroral hiss events observed by DE 1 at high altitudes probably originate as upward propagating auroral hiss emissions known as saucers, which are observed with low-altitude polar-orbiting satellites [*Gurnett and Frank*, 1972; *James*, 1976]. Both upward and downward propagating saucer emissions are commonly observed at low altitudes in the auroral zone [*Horita and James*, 1982].

It has long been known that auroral hiss is closely associated with low-energy auroral electron beams [*Gurnett*, 1966; *Gurnett and Frank*, 1972; *Laaspere and Hoffman*, 1976]. Prior to DE 1 all of the auroral hiss and low-energy electron comparisons were made with low-altitude satellites. These observations showed that the downward propagating auroral hiss is closely related to downward moving "inverted-V" electrons. Since auroral hiss is believed to be produced by a Landau resonance [*Maggs*, 1976] in which the electron beam moves in the same direction as the wave, i.e., $\omega/k_{\parallel} \simeq v_b$, the upward propagating auroral hiss detected by DE 1 is expected to be associated with upward moving electrons. A search for such upward directed electron beams was performed by *Lin et al.* [1984] using DE 1, and several events were found in which upward moving electron beams were associated with funnel-shaped auroral hiss emissions. These electron beams were found to have a peak energy around 50 eV, a temperature of about 20 eV, and a density of the order of 1 cm^{-3}. Ray path studies of specific cases showed that the lower boundary of the auroral hiss source is located at an altitude of about 1 R_E. The existence of a low-altitude limit to the auroral hiss source suggests that the electron beam acceleration may occur at this altitude. These source altitudes are in good agreement with the altitude of the electron acceleration region estimated by *Burch et al.* [1983] on the basis of electron pitch angle distributions.

In contrast to the auroral hiss, much less is known about the origin and propagation of Z mode radiation over the auroral zone and polar cap. The Z mode is a very complicated plasma wave mode. As can be seen from Figure 4, the bandwidth of the Z mode is a very sensitive function of the ratio of the electron plasma frequency to the electron cyclotron frequency. When f_{pe}/f_{ce} is greater than 1, the bandwidth is very

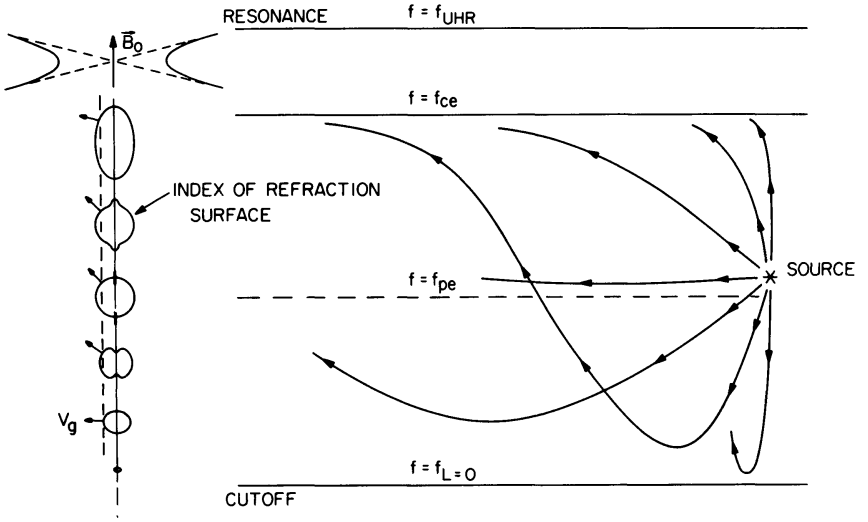

Fig. 17. A qualitative analysis of the ray path of Z mode radiation for the special case of a vertical magnetic field in a horizontally stratified plasma. The Z mode radiation is reflected as it approaches the $f_{L=O}$ cutoff and asymptotically approaches the level where $f = f_{ce}$. If the magnetic field is tilted away from vertical, or if horizontal gradients are present, the radiation can enter the region above $f = f_{ce}$ but can never propagate beyond $f = f_{UHR}$.

narrow, whereas when f_{pe}/f_{ce} is less than 1, the bandwidth is very broad. This dependence explains why the broadband Z mode emissions are not observed in other parts of the magnetosphere. It is only in the very low density regions found at high altitudes over the auroral zone and polar cap that the f_{pe}/f_{ce} ratio is sufficiently small for large bandwidths to occur. In most other regions of the magnetosphere the bandwidth of the Z mode is very narrow: $\Delta f/f$ of about few percent. The resulting narrow-band emissions are usually called upper hybrid resonance (UHR) emissions. The peak intensities usually occur near the upper hybrid resonance frequency, which is at the upper edge of the band. Upper hybrid emissions are usually considered a "local" emission because the narrow bandwidth confines the waves to a very restricted spatial region.

Because of the broad bandwidth of the Z mode in the low-density region over the auroral zone and polar cap, the radiation can propagate over large distances, both horizontally and vertically. The general nature of the propagation can be understood by considering the shape of the index of refraction surface as a function of altitude. The index of refraction surface is indicated schematically in Figure 17 for altitudes ranging from cutoff at $f = f_{L=O}$ to resonance at $f = f_{UHR}$. The topology of the index of refraction surface changes at the electron cyclotron frequency. Above the electron cyclotron frequency the index of refraction has a resonance cone, with no propagation from 0 to θ_{res}. Below the electron cyclotron frequency, propagation is allowed for all wave normal angles, and the index of refraction surface has a more or less elliptical shape. The index of refraction surface shrinks to zero radius at cutoff, $f = f_{L=O}$, and expands to an elongated ellipsoid along the magnetic field as f approaches f_{ce} from below. For a detailed description of the index of refraction surface of the Z mode, see *Budden* [1961].

To analyze the Z mode propagation, one can use a simple Poeverlein construction [*Poeverlein*, 1949]. To a first approximation the medium is assumed to be horizontally stratified with the magnetic field vertical, as it would be over the polar region. Snell's law then shows that the horizontal component of the index of refraction, $n \sin \theta$, is constant. A representative constant value for $n \sin \theta$ is indicated by the vertical dashed line through the index of refraction surfaces on the left side of Figure 17. The group velocity at each altitude is then given by the normal to the index of refraction surface at the intersection with the dashed line, as indicated by the arrows. Using these group velocity directions, the ray path can then be sketched starting at various source positions and wave normal angles. A representative series of ray paths is shown on the right of Figure 17. The general trend is quite clear. Rays with initial wave normal angles directed upward asymptotically approach the level where $f = f_{ce}$. For an exactly vertical magnetic field, these rays cannot reach the level above $f = f_{ce}$. However, if the magnetic field deviates from vertical, or if horizontal gradients are present, some penetration can occur into the region above $f = f_{ce}$. Rays with initial wave normal angles directed downward are reflected as they approach the cutoff at $f = f_{L=O}$. After reflection the ray asymptotically approaches the level where $f = f_{ce}$.

The simple ray path model shown in Figure 17 explains many of the characteristic features of the Z mode radiation. The ability of the radiation to propagate horizontally with relatively little refraction, except near $f_{L=O}$ and f_{ce}, explains why the radiation is detected over a large region of the polar cap, even though the auroral zone is the most likely source. In considering possible source locations, there is presently very little direct evidence from DE 1 to indicate exactly where the radiation is generated. The wideband data show that the spectrum is relatively smooth and continuous, like auroral hiss, and not at all like auroral kilometric radiation, which has considerable fine structure [*Gurnett et al.*, 1979]. Recent direction-finding studies by *Hashimoto et al.* [1987] indicate that the Z mode radiation is generated in the auroral zone and may originate from auroral hiss via a coupling window that occurs near the electron plasma frequency.

5. Myriametric (Continuum) Radiation and Equatorial UHR Emissions

Terrestrial myriametric radiation (TMR) consists of radio emissions with wavelengths of tens of kilometers (myriametric) that are generated by intense upper hybrid emissions near the plasmapause. Myriametric radiation has also been called continuum radiation by *Gurnett* [1975] and *Gurnett and Frank*

[1976], who provided the first evidence that the radiation is generated by electrostatic oscillations near the electron plasma frequency. Later, several investigators, including *Rönnmark et al.* [1978] and *Kurth et al.* [1979], showed that the electrostatic waves were at the upper hybrid resonance frequency. The free-energy source for the upper hybrid resonance waves is believed to be a loss cone anisotropy in the trapped electron distribution. Path-integrated growth rate calculations show that the favored region for the growth of these waves is near the equatorial plane. Myriametric radiation was originally called continuum radiation because it appeared to have a continuous frequency spectrum, similar to trapped continuum radiation [*Gurnett and Shaw*, 1973]. However, more recent high-resolution spectral measurements clearly show that the radiation is not continuous but instead consists of many closely spaced lines [*Kurth et al.*, 1981]. For this reason and other reasons, *Jones* [1982] suggested that the escaping continuum radiation should be renamed terrestrial myriametric radiation.

Several theories have been advanced to explain the conversion of the locally generated UHR emissions to escaping myriametric radiation. These theories can be categorized as linear and nonlinear. The linear mechanism was proposed by *Jones* [1976], who suggested that UHR emissions, which are in fact Z mode waves, are converted to escaping left-hand-polarized ordinary (L-O) mode waves via a tunneling process. This linear tunneling process is well known in ionospheric radio propagation and is usually referred to as the "radio window" [*Budden*, 1961]. The radio window is located at the electron plasma frequency and occurs whenever the plasma density gradient is sufficiently steep to make the gap between the Z mode and the L-O mode comparable to or smaller than a wavelength. Several nonlinear mode conversion mechanisms also exist, all of which require wave-wave interactions to produce the escaping electromagnetic radiation. These theories have been reviewed by *Melrose* [1981]. At present the favored nonlinear mechanism involves the interaction of an upper hybrid resonance wave with a low-frequency electrostatic wave to produce the escaping electromagnetic radiation.

The linear conversion theory of *Jones* [1976, 1980] provides two predictions that the DE 1 plasma wave instrument is ideally suited to test. The first prediction is that the myriametric radiation should be beamed outward in two meridional beams at angles of $\pm\gamma$ with respect to the magnetic equator as shown in Figure 18. The angle γ is given by

$$\gamma = \arctan\,(f_{ce}/f)^{1/2} \tag{4}$$

where the electron cyclotron frequency is evaluated at the escape point. Since DE 1 provides north-south passes through the magnetic equator, this spacecraft has an ideal orbit required for observing the predicted beaming. For an equatorial plasmapause source, the best viewing geometry occurs when the apogee is near the equator, which occurs approximately once every 20 months. The second prediction is that the radiation should be left-hand polarized with respect to the magnetic field in the source region (i.e., L-O mode). The polarization measurement capability of DE 1 also provides an opportunity to verify this prediction.

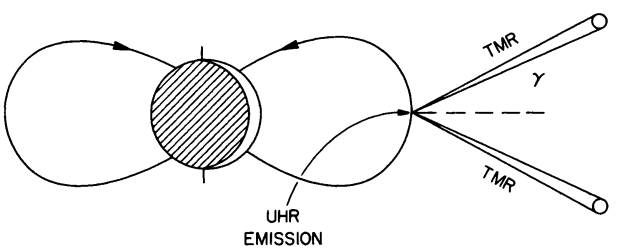

Fig. 18. A qualitative sketch showing the beaming of myriametric radiation away from an equatorial source as predicted by *Jones'* [1976] "radio window" model. The beam angle γ can be directly measured by a spacecraft passing from north to south outside the plasmasphere.

The equatorial beaming of the terrestrial myriametric radiation has been investigated using the DE 1 data by *Jones et al.* [1987]. A spectrogram of a myriametric radiation event detected by DE 1 during a south to north pass through the magnetic equator is shown in Figure 19. The myriametric radiation appears as two distinct bursts (labeled TMR) from about 60 to 100 kHz. These two bursts occur symmetrically with respect to the magnetic equator (λ at the bottom of the plot gives the magnetic latitude). An intense electrostatic emission can also be seen at the upper hybrid resonance frequency, which in this case is $f_{UHR} \simeq 62$ kHz. This UHR emission is not the source of the myriametric radiation, since the escape region must lie earthward of the spacecraft. However, it does demonstrate that equatorial UHR emissions were present during this pass. Direction-finding measurements performed on the two bursts of myriametric radiation are shown at points A and B in Figure 20. These measurements show directions of arrival that are in good qualitative agreement with the beaming model shown in Figure 18. The radiation appears to be arriving from the $L = 4.0$ magnetic field line at a point slightly south of the magnetic equator. The $L = 4.0$ field line is a very reasonable location for the plasmapause during this pass. Furthermore, the arrival directions, δ and γ, are within a few degrees of the arrival directions predicted with equation (4). Unfortunately, for this case the intensity of the myriametric radiation was not high enough to make polarization measurements. However, a recent study of a more intense event by *Gurnett et al.* [1988] shows the expected L-O mode polarization.

Overall, the DE 1 measurements provide very strong support for the linear conversion model of *Jones* [1980]. Although these measurements do not rule out the possibility of a nonlinear conversion mechanism, to date no nonlinear mechanism has been proposed that provides predictions which fit the observations as well as the linear conversion mechanism.

6. Whistler Mode Waves and Wave Particle Interactions

In the inner magnetosphere, on closed field lines at $L < 7$, whistler mode wave particle interactions establish high levels of whistler mode "noise," including spontaneously generated chorus and hiss emissions and triggered emissions that have their origin in lightning-generated whistlers, VLF transmitter signals, and power line radiation. It is widely agreed that whistler mode wave-particle interactions play a dominant role in the acceleration and loss of energetic radiation belt electrons [*Lyons and Williams*, 1984]. However, much remains to be learned about the relative contributions to this loss by magnetospheric waves of different origin [*Imhof et al.*, 1984, 1986]. For example, it is known that both spontaneous and whistler-triggered chorus bursts can induce detectable precipitation of energetic particles outside the plasmasphere [*Rosenberg et al.*, 1971; *Helliwell et al.*, 1980]. Throughout the inner magnetosphere, lightning-generated whistlers are now known to

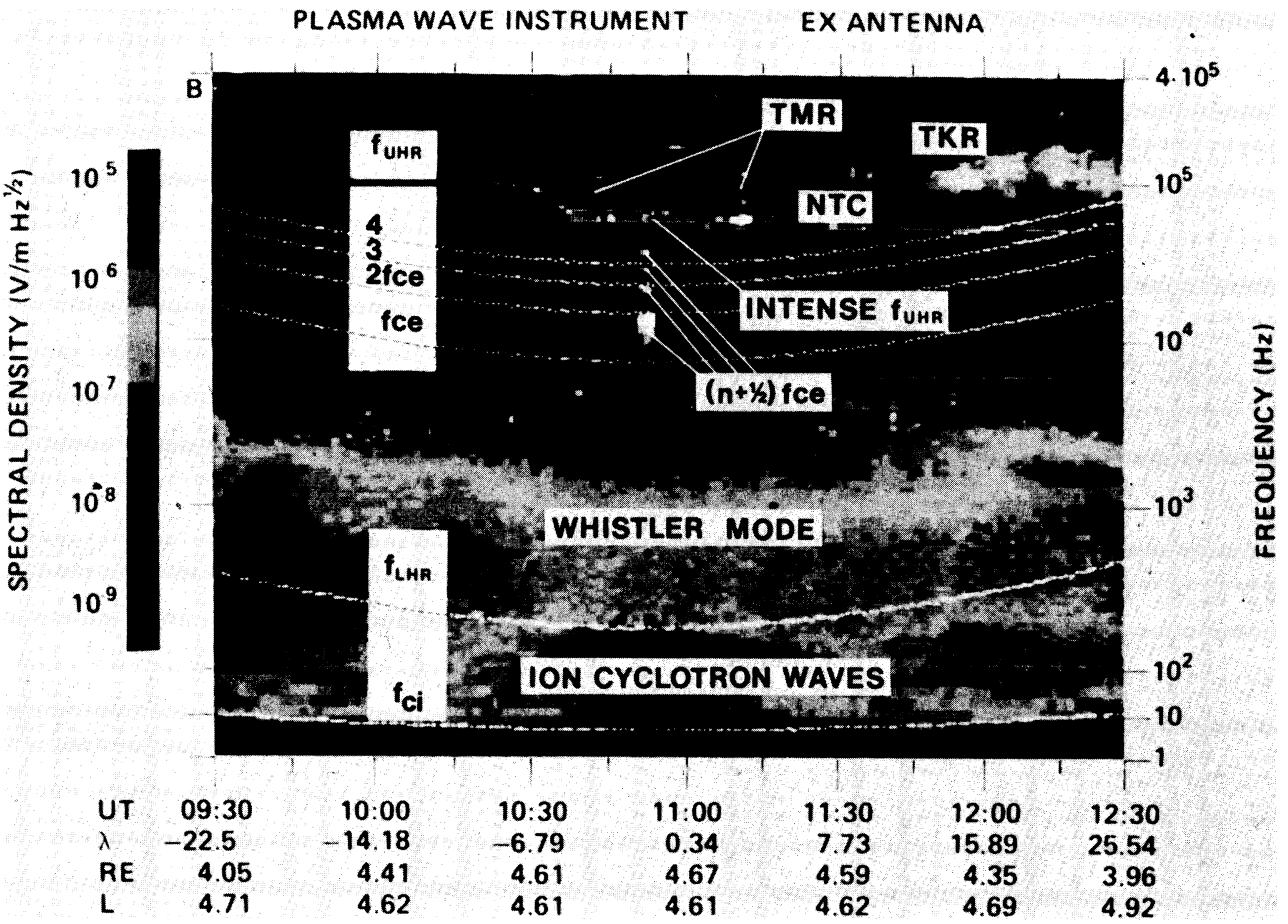

Fig. 19. A south to north DE 1 pass through the magnetic equator showing the two bursts of terrestrial myriametric radiation (TMR) predicted by Jones' beaming model north and south of the equator [from *Jones et al.*, 1987].

induce bursts of electron precipitation [*Helliwell et al.*, 1973; *Carpenter and LaBelle*, 1982; *Inan et al.*, 1985; *Voss et al.*, 1984; *Goldberg et al.*, 1986; *Inan and Carpenter*, 1986, 1987]. Recent satellite experiments, involving controlled injection of waves from a ground-based VLF transmitter, have also provided the first direct evidence of the precipitation of trapped radiation belt particles by man-made radio waves [*Imhof et al.*, 1983*a*, *b*; *Kovrazhkin et al.*, 1984]. However, the relative contributions to precipitation by ducted versus nonducted forms of these waves are not yet known, and their relative importance with respect to other waves such as ELF hiss has not been evaluated.

The DE 1 satellite, with its polar orbit and apogee of ~4.6 R_E, is well suited to contribute to the resolution of these questions by means of comprehensive in situ measurements of the relevant whistler mode wave spectrum. An example of a 2- to 25-kHz spectrum measured near the equatorial plane in the inner radiation belt at $L \simeq 1.6$ is shown in Figure 21. In the frequency range shown, multiple whistlers arrive over a direct (half hop) path with intense wave energy extending up to 25 kHz. In a few cases, more dispersed whistler components also arrive at the satellite, presumably after reflection from the ionosphere or within the magnetosphere, with significant wave energy up to ~15 kHz. At lower frequencies (<2 kHz), there is plasmaspheric hiss at an intensity lower than that of the whistlers, as evidenced by the fact that the automatic gain control (AGC) of the receiver is dominated by the whistlers during the times they are observed. Also seen in Figure 21 are

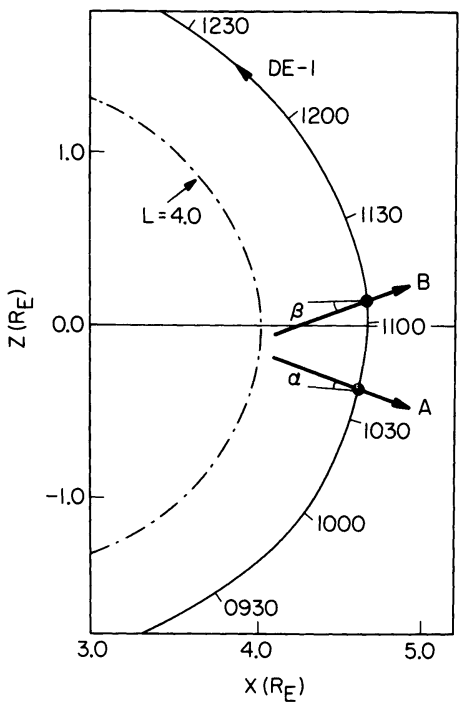

Fig. 20. Direction-finding measurements for the event in Figure 19 showing that the terrestrial myriametric radiation originates from near the magnetic equator. The ray path angles are in good quantitative agreement with the directions predicted by Jones' beaming model [from *Jones et al.*, 1987].

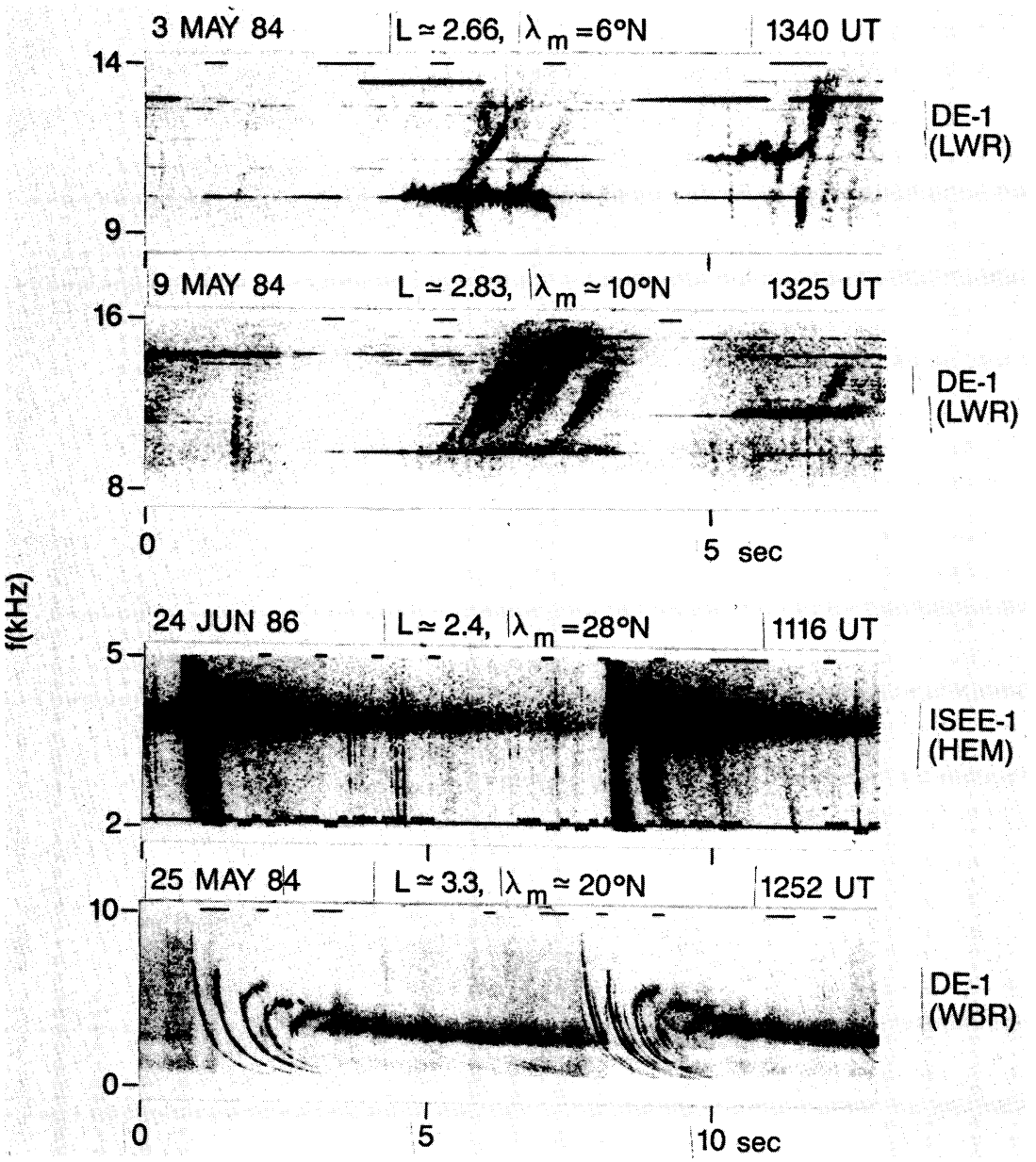

Fig. 22. Whistlers and Omega transmitter signals observed on ISEE 1 and DE 1. The upper two panels show discrete emissions triggered by transmitter pulses propagating in the nonducted mode. A distinctly different character appears (second panel from top), in comparison to emissions triggered by ducted signals observed on the ground [*Bell et al.*, 1981]. The bottom panel shows magnetospherically reflected whistlers; each sequence is generated by a single lightning flash. The second panel from the bottom shows lower hybrid resonance noise bursts triggered by whistlers, with the emission band enduring for up to 5–10 s, much longer than the observed duration of the triggering signal.

is accompanied by emissions. The second panel shows another example, in which the emissions are again associated with later arriving pulses. The spectral characteristics of these emissions (e.g., high df/dt, presence of successive, sometimes overlapping elements) are distinctly different from those triggered by ducted signals observed on the ground [*Bell et al.*, 1981]. The bottom panel of Figure 22 shows two successive whistler events observed on DE 1 near $L \simeq 3.3$. Each event is triggered by a single lightning flash and consists of a sequence of traces that arrive at the satellite after undergoing successive magnetospheric reflections [*Edgar*, 1976]. During the time of the whistler events, no other significant wave activity is seen in the 0- to 10-kHz range, as evidenced by the fact that the receiver AGC is dominated by the whistler signal. The second panel from the bottom shows lower hybrid resonance (LHR) noise bursts repeatedly triggered by whistlers, with the emission bands enduring for up to 5–10 s, much longer than the observed duration of the triggering whistler.

In addition to the observation of the equatorial regions within the radiation belts at $L < 3$, the DE 1 orbit allows for convenient study of whistler mode wave activity in the vicinity of the plasmapause. Data from a typical ~2-hour crossing of this region, acquired during controlled VLF wave injection experiments with the Siple Station, Antarctica, transmitter, is shown in Figure 23, together with a meridional plane projection of the relevant orbital segment. Samples of the spectrum

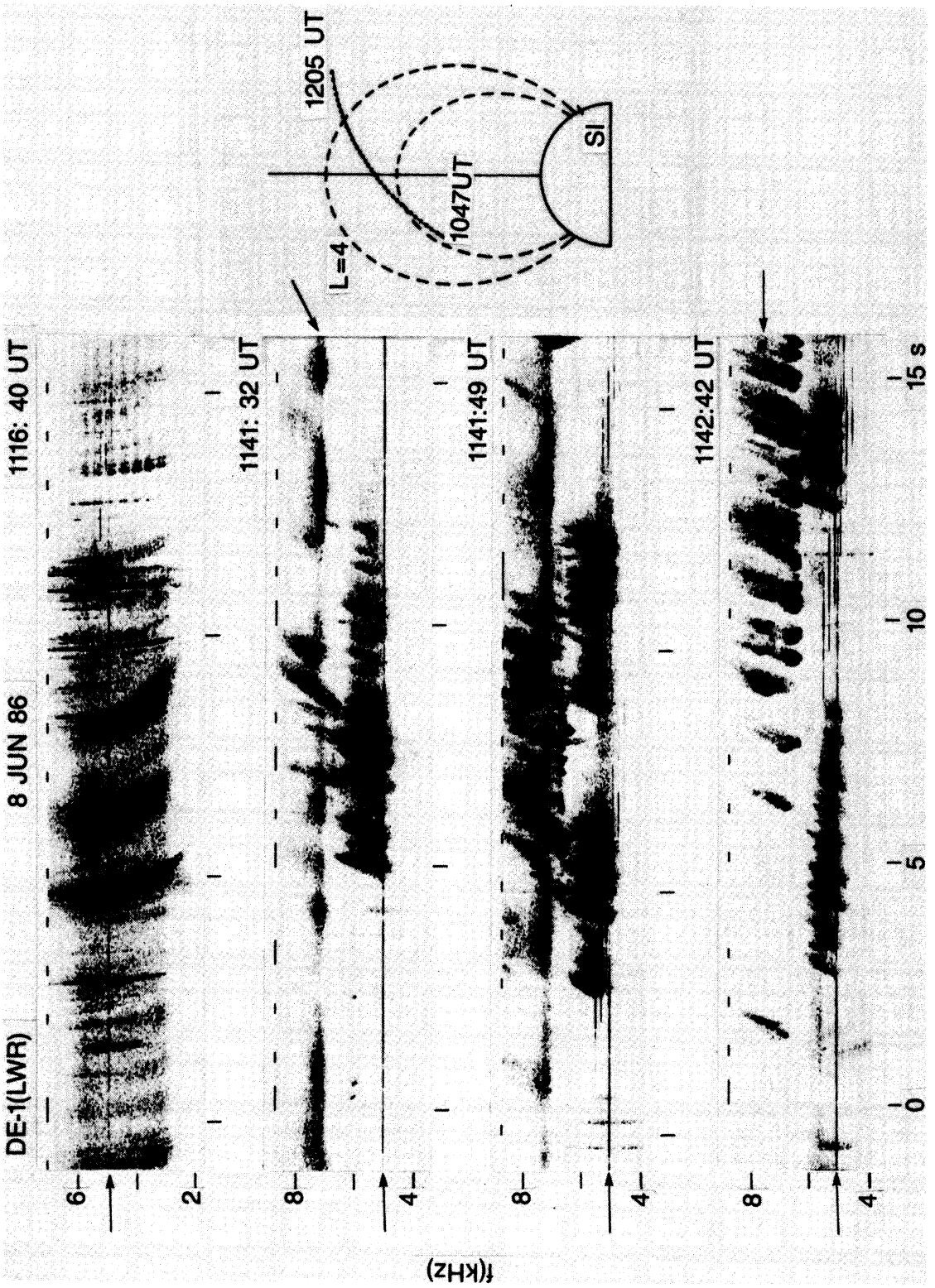

Fig. 23. Whistlers, natural emissions, Siple transmitter signals, and triggered emissions observed on the DE 1 satellite. The meridional plane projection of the satellite orbit is shown on the right. The transmitted format is not shown separately but consists of a nonoverlapping sequence of continuous wave transmissions at the center frequency indicated by the arrows at the left and 1-s pulses at other frequencies within a ± 500-Hz bandwidth around the center frequency. The signals received on the satellite show significant overlap of the pulses, due to a combination of multipath propagation and echoing. The arrows at the right point to natural emission bands.

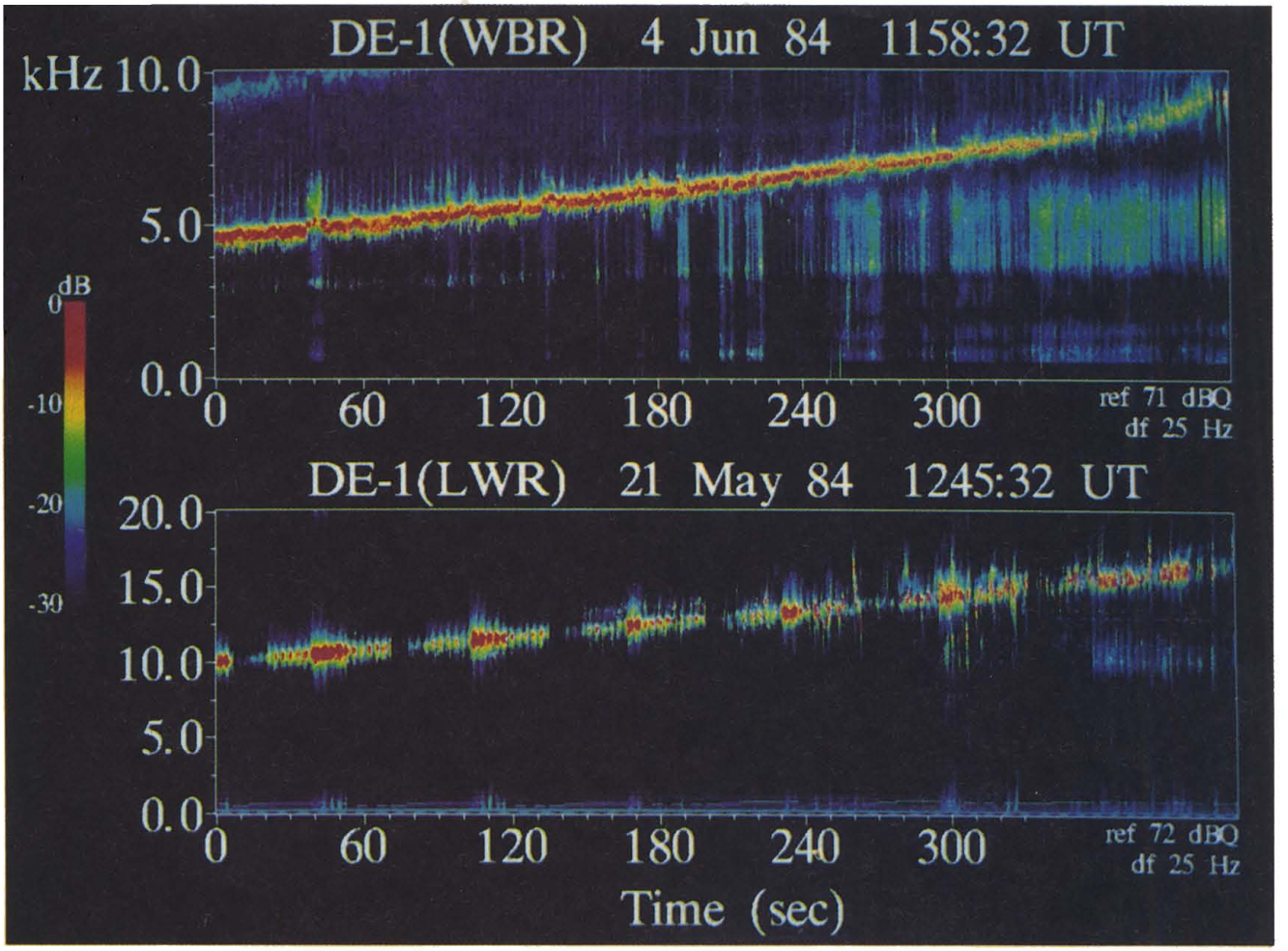

Fig. 24. Examples of discrete emission bands observed on the high-altitude DE 1 satellite. Data from two different periods in which the DE 1 orbital configuration was similar are shown. The upper panel shows data from the WBR (600 Hz to 10 kHz). The lower panel shows data from the 10- to 16-kHz band of the LWR. LWR toggles between the E_x and B antennas every 32 s and has a steep roll-off above 16 kHz (~10 dB down at 17 kHz) [*Poulsen and Inan*, 1988].

in the 2- to 8-kHz range are shown at four different times when the satellite was near the vicinity of the geomagnetic equator. In the top panel we see whistlers and the Siple transmitter signals without any associated emission activity. The high rate of observed whistler activity is typical of conditions inside the plasmasphere [*Carpenter et al.*, 1968]. Later during the same pass, the whistler activity terminated abruptly (typical of plasmapause crossings), and both natural and Siple signal–triggered emission activity was observed as shown in the lower three panels. The relatively steady band of emissions near ~7 kHz decreased in frequency as the satellite moved to higher L shells, typical of magnetospheric chorus [*Burtis and Helliwell*, 1976].

Natural Waves: Hiss and Chorus

DE 1 observations in the inner magnetosphere at $L < 3$ have led to the identification of a new type of discrete whistler mode emission occurring at middle to low latitudes [Poulsen and Inan, 1988]. Examples of these emission spectrums are illustrated in Figure 24. In summary, the emission elements are confined to a bandwidth of 1–5 kHz, with the lower cutoff frequency of the band varying with L shell, being equal to ~0.2–0.5f_c(Eq), where f_c(Eq) is the equatorial electron cyclotron frequency. The discrete and burstlike nature of the emissions is similar to that of chorus emissions typically observed at higher L; however, dispersion of individual elements is often different from typical chorus, and the emissions are observed inside as well as outside the plasmapause. The phenomenon seems to occur mainly in the early morning local time sector (0400–0800 MLT) and is well correlated with geomagnetic activity, occurring mostly when $\Sigma Kp > 30$. The analysis of data from the low-altitude ISIS 2 and the high-altitude DE 1 satellites indicates that the emissions may be generated near the equatorial plane at frequencies of ~0.2f_c(Eq) inside and ~0.35f_c(Eq) outside the plasmapause. The parallel energy of electrons for cyclotron resonance with the observed wave is found to be ~20–50 keV in both cases. Observations in the vicinity of low-altitude crossings of the plasmapause also indicate the presence of a second emission band, which is interpreted to result from reflection of the equatorially generated emissions from the lower ionosphere.

In a study of whistler mode chorus emissions using simultaneous data from Halley Bay and Siple stations in the Antarctic and from DE 1, it was shown that individual emission elements observed on the satellite were predominantly the

result of downward ducted propagation followed by a reflection at low altitude, with the signals subsequently reaching the satellite in the nonducted mode [*Smith et al.*, 1985]. Such a "hybrid" mode of propagation (see Figure 25) provides a means by which signals generated, amplified, or triggered in small localized ducts can spread into much larger regions of the inner magnetosphere.

A detailed investigation of the wave normal direction and spectral properties of whistler mode hiss was carried out using LWR data from DE 1 [*Sonwalkar and Inan*, 1988]. A new formalism to analyze satellite data allowed the representation of the hiss by a field distribution function (FDF), in terms of which the observed data were interpreted. Using spin modulation of the hiss intensity as observed with the electric and magnetic antennas over an extended ($\sim$3-hour) period, it was determined that the hiss emissions were generated with wave normal angles at an angle of 30°–80° with respect to the magnetic field, but also nearly perpendicular to the meridional plane.

Siple/DE 1 VLF Wave Injection Experiments

During the periods when the apogee of the DE 1 orbit was in the vicinity of the magnetic equatorial plane, controlled wave injection experiments were conducted using the Siple Station, Antarctica, VLF transmitter facility.

Figure 25 shows the simultaneous reception of Siple transmitter signals on the ground at Roberval and on the DE 1 satellite. The bottom panel shows the frequency-time format of transmissions, the middle panel the dynamic spectrum of the signals received on DE 1 using the magnetic antenna, and the top panel the spectrum of the receptions at Roberval. All records are aligned in absolute time so that the ground-to-ground and ground-to-satellite time delays can be seen. In this case the transmitter signals are first seen on the satellite, then at Roberval, and then again on the satellite following reflection from the lower ionosphere. This process is depicted in the schematic panel of Figure 25 and is called the hybrid mode of propagation, since it involves initial ducted propagation, followed after ionospheric reflection by nonducted propagation. Analysis of the time delay variation and ray tracing in a model magnetosphere (using in situ cold plasma density from UHR frequency and also ground-based whistler data) confirmed the predominance of the hybrid propagation mode [*Rastani et al.*, 1985]. The importance of the hybrid mode of propagation in this case lies in the spatial and temporal extent of the signal reception. As mentioned above in connection with chorus emissions, this mechanism allows for large regions of the magnetosphere to be populated by waves that are either regenerated or amplified in ducts. These waves subsequently propagate in a nonducted mode following reflection from the lower ionosphere.

Another example of emissions triggered by signals from the Siple Station, Antarctica, transmitter is shown in Figure 26. The lower panel shows the transmitted format, consisting of a staircase of nonoverlapping 1-s-long pulses at different frequencies, aligned in absolute time with the dynamic spectra of the signal received on DE 1 as shown in the upper panel. For the case shown, the radiated power from the transmitter was maximized (through tuning) at 2.45 kHz, as is evident from the format panel in Figure 25. The emission burst is triggered by the transmitter pulse at 2.2 kHz and endures for many seconds beyond the termination of the triggering pulse. The time delay for the first arriving signal components is $\sim$1.4 s. Ray tracing on the basis of cold plasma density as measured on the satellite (UHR) as well as on the ground (whistlers) indicates that the observed signals propagated in the ducted mode followed by a nonducted path after reflection from the lower ionosphere in the north (i.e., the hybrid mode as discussed above in connection with Figure 24).

Observations of Siple transmitter signals near the geomagnetic equatorial plane on the DE 1 satellite were used to determine the wave propagation direction of the signals, as well as to provide a first estimate of the effective length of an electric dipole antenna in the magnetosphere [*Sonwalkar and Inan*, 1986]. Interpretation of the spin modulation characteristics observed on a continuous wave pulse alternately with the electric and magnetic field antennas indicated that the transmitter signals were propagating at an angle of $\sim$50° with respect to the magnetic field, consistent with that expected on the basis of ray tracing. Using in situ (UHR) measurements of the electron density, and also the magnetic field measurements, the effective length of the 200-m tip-to-tip electric dipole antenna was estimated to be 230 $\pm$ 50 m, roughly twice the length that is commonly assumed. Since the inner 71.1-m section of each 100-m element is covered with an insulator [*Shawhan et al.*, 1981], one possible explanation is that the antenna is still operating in the resistive "dc mode" at VLF frequencies. The center-to-center distance between the conducting part of the elements is 173.1 m, which is comparable to the effective length obtained from the magnetic field comparisons. Similar (unpublished) comparisons have also been made at higher frequencies ($\sim$100 kHz) using auroral kilometric radiation. At these higher frequencies the effective length is within about 10% of one-half the tip-to-tip length, which is the value expected in the capacitive "ac mode." Apparently, the transition from "dc" to "ac" coupling occurs at frequencies of a few tens of kilohertz. The transition frequency probably depends on the electron density and other parameters. At present, no systematic study of the transition frequency has been performed.

Spectral Broadening: Stimulated Electrostatic Waves

In addition to the well-known whistler mode wave-particle interactions apparently occurring at high altitudes near the equatorial plane, a new kind of interaction has recently been discovered at low altitudes ($<$8000 km) [*Bell et al.*, 1983]. This phenomenon, termed "spectral broadening," involves the generation of sideband electrostatic waves as originally narrow-band ($\sim$1 Hz) signals propagate through the ionosphere to altitudes of 600–8000 km. The effect has been observed in recent data from the ISIS 1, ISIS 2, ISEE 1, DE 1, ARCAD 3, and InterCosmos 19 satellites [*Inan and Bell*, 1985; *Titova et al.*, 1984; *Tanaka et al.*, 1985; *Bell and Ngo*, 1988] and appears to involve the scattering of electromagnetic waves from irregularities that are created and maintained by energetic particle precipitation from the magnetosphere. Electrostatic waves are excited and amplified, and pitch angle scat-

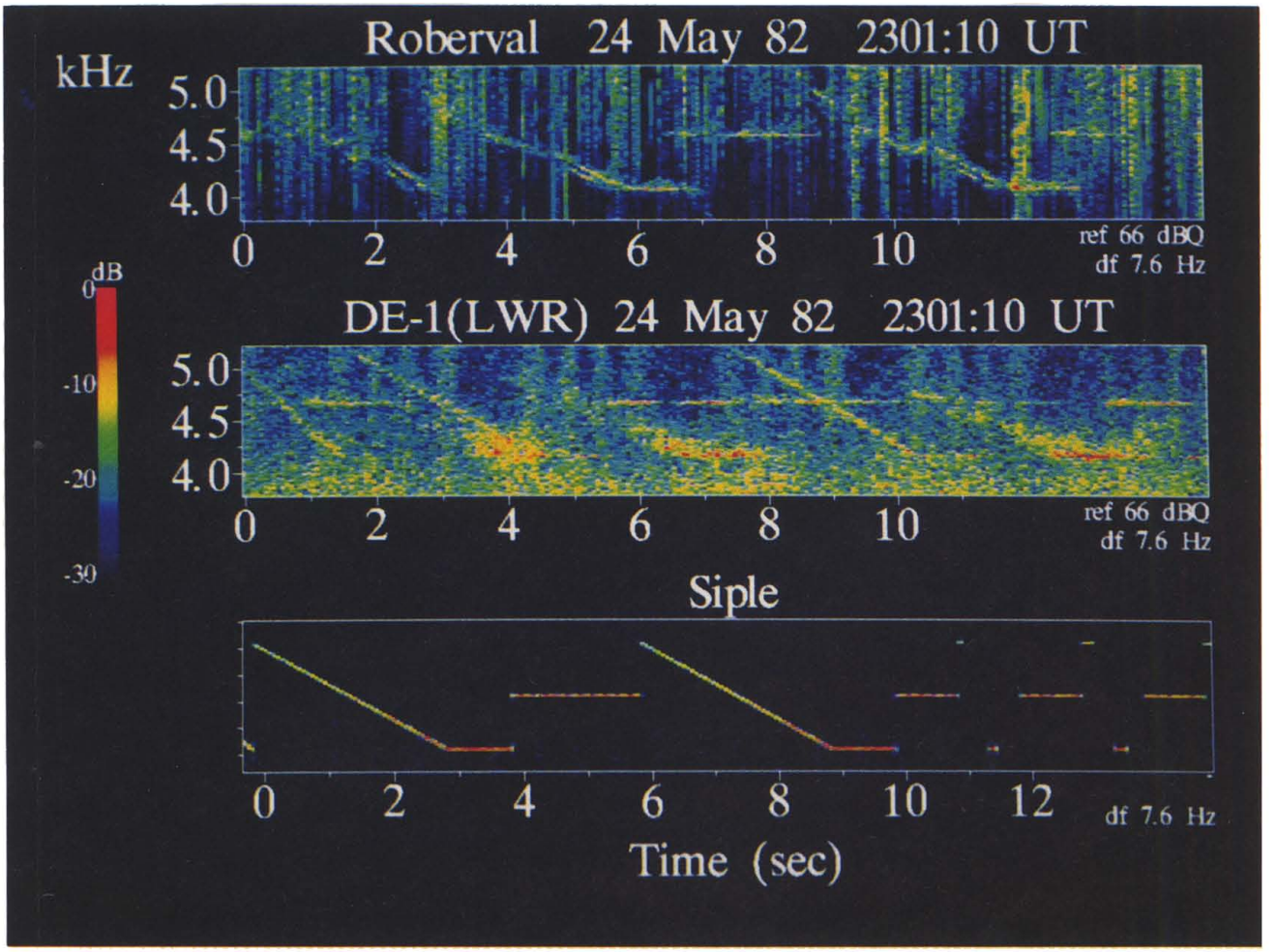

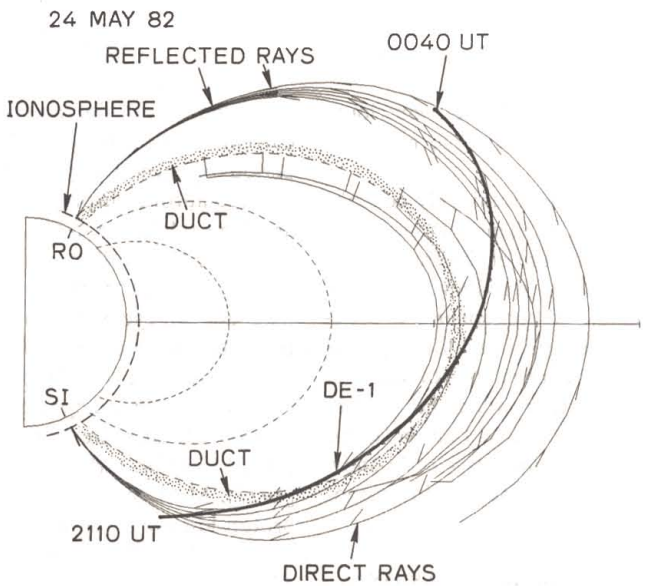

Fig. 25. Simultaneous reception of Siple transmitter signals at Roberval, Quebec, Canada (conjugate to Siple Station) and on the DE 1 satellite. The lower panels show the transmitter format. All panels are aligned in absolute time. The first signal to arrive at the satellite (located near the equatorial plane) was interpreted to have propagated in the nonducted mode. Signal components that are presumed to have propagated in a magnetospheric duct are observed subsequently at Roberval. Ducted signal energy reflected from the lower ionosphere then propagates upward to the satellite location in the nonducted mode. This mode of propagation is termed the "hybrid" mode [*Rastani et al.*, 1985] and is schematically described in the bottom part of the figure.

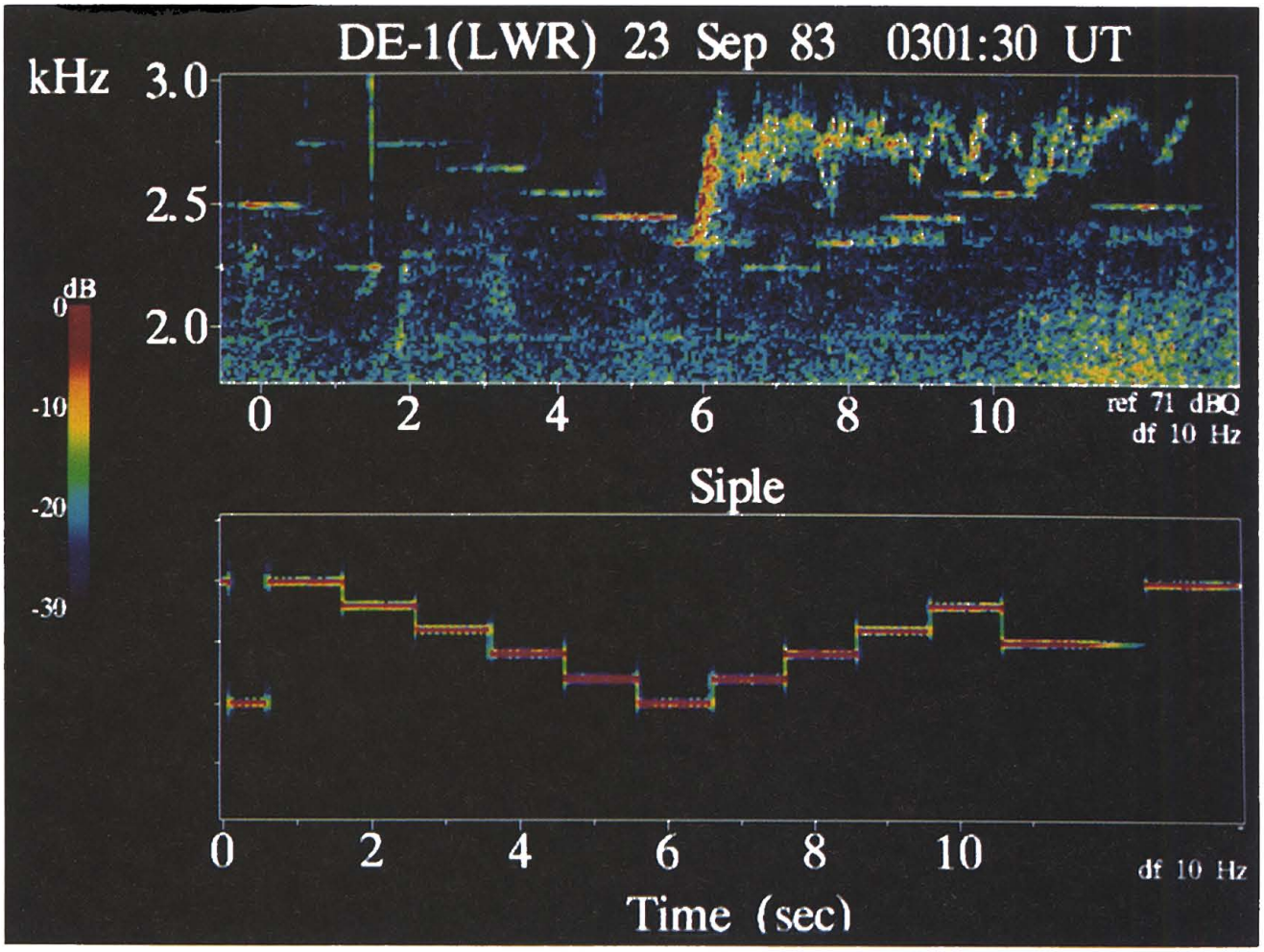

Fig. 26. Emission triggering by Siple transmitter signals. The lower panel shows the transmitted signal aligned in absolute time with the spectrum received on DE 1 that is shown in the upper panel. For the case shown, the radiated power from the transmitter was maximized (through tuning) at 2.45 kHz. The emission burst is triggered by the transmitter pulse at 2.2 kHz and endures for many seconds beyond the termination of the triggering pulse.

tering of the energetic electrons occurs which may contribute significantly to the loss of the electrons from the radiation belts.

Observations on the DE 1 satellite have uniquely contributed to the understanding of this new phenomenon by establishing the primarily electrostatic nature of the effect [*Inan and Bell*, 1985]. Figure 27 shows the first simultaneous observation of the electric and magnetic field components of spectrally broadened signals on DE 1. The upper and lower panels show the 13.1-kHz signal from the Omega, North Dakota, transmitter. The arrow indicates the time when the receiver was switched from magnetic (B) to electric (E_x) antennas (or vice versa). While the electric field components clearly show broadening by as much as 130 Hz, the magnetic field components have a bandwidth of less than 10 Hz.

7. Equatorial Ion Cyclotron and Ion Bernstein Mode Emissions

For many years there has been considerable interest in low-frequency electromagnetic emissions associated with energetic ions trapped near the magnetic equator. During magnetic storms, ions are injected into the inner regions of the magnetosphere producing an east-west current known as the ring current. This injected ion distribution typically decays over a period of several days and is often associated with a low-latitude auroral display known as a stable auroral red (SAR) arc. To explain the decay of the equatorially trapped ion distribution, *Cornwall et al.* [1970] first suggested that the ring current ion distribution is unstable to the growth of electromagnetic ion cyclotron waves in the high-density region inside the plasmasphere and that these waves scatter particles into the atmosphere, thereby causing the aurora. Observations of electromagnetic ion cyclotron waves produced by ring current ions have been made by several groups, including *Taylor et al.* [1975], *Taylor and Lyons* [1976], and *Kintner and Gurnett* [1977]. Most of the early observations were associated with proton ion cyclotron waves, which in the vicinity of the plasmapause have frequencies in the range around 10 Hz. Later, when it was recognized that the ring current ion distribution also contained heavier ions, such as He^+ and O^+ [*Williams*, 1980], the emphasis shifted to the study of ion cyclotron waves associated with the heavier ions, which have frequencies in the range around 1 Hz or less [*Gendrin and Roux*, 1980; *Gendrin*, 1981; *Mauk et al.*, 1981]. These studies showed that

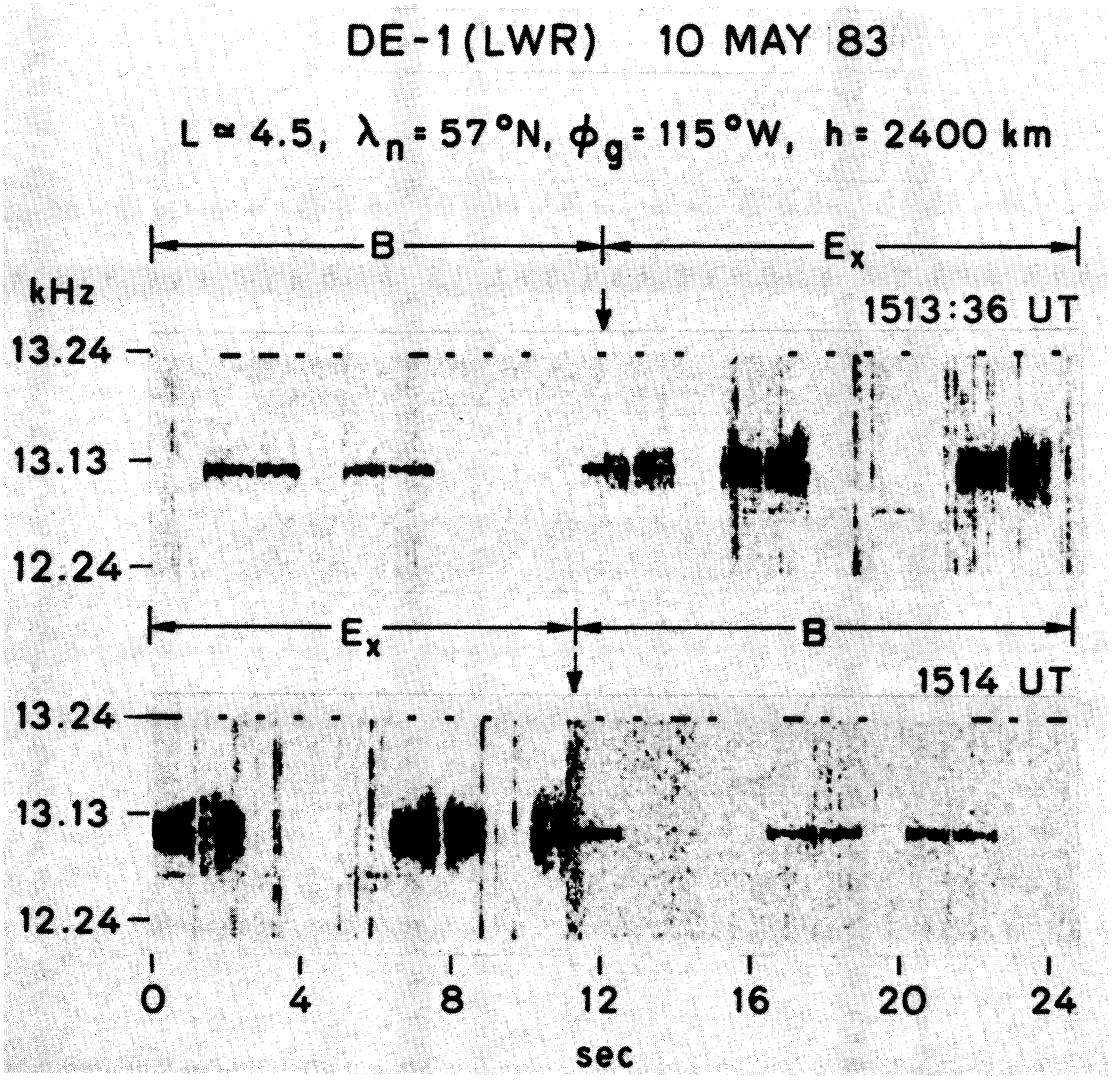

Fig. 27. Electric (E_x) and magnetic (B) field components of spectrally broadened 13.1-kHz Omega transmitter signals observed at low altitudes on the DE 1 satellite. Substantial (~130 Hz) broadening of the signal is apparent in the electric field, but the magnetic field components have a bandwidth of less than ~10 Hz [*Inan and Bell*, 1985].

electromagnetic ion cyclotron waves play an important role in the energy transfer between various ion species in the ring current.

In addition to the electromagnetic ion cyclotron waves another class of waves, known as electromagnetic ion Bernstein mode emissions, has been associated with equatorial ion distributions. These waves were first identified by *Russell et al.* [1970], who showed that an intense band of electromagnetic noise sometimes occurred near the magnetic equator at frequencies from about 10 to 100 Hz. Later, *Gurnett* [1976] showed that the equatorial noise consisted of many narrowband emissions near harmonics of the H^+, He^+, and O^+ ion cyclotron frequencies. The existence of ion cyclotron harmonic effects provided strong evidence that the waves are of a general class known as the electromagnetic ion Bernstein modes [*Fredricks*, 1968]. More recently, *Olsen* [1981] showed that the equatorial ion Bernstein mode emissions are closely related to a highly anisotropic low-energy, 20- to 50-eV, ion population that is present near the equatorial plane. In contrast to the ion cyclotron waves, the ion Bernstein mode emissions occur during magnetically quiet times, as well as disturbed times. Typically, the ion Bernstein mode events last a few days to a week and then gradually disappear. Such events occur a few times per year.

Since DE 1 crosses the magnetic equator twice per orbit at radial distances ranging out to 4.65 R_E, this spacecraft provides a good opportunity for studying both the electromagnetic ion cyclotron waves and the electromagnetic ion Bernstein waves. Relatively few ion cyclotron wave events have been found in the DE 1 data. Approximately one-half dozen events occurred over a 3-year period. This occurrence rate is similar to that reported by *Kintner and Gurnett* [1977] using similar types of sensors but is considerably smaller than the rate reported by *Roux et al.* [1982] using GEOS data. The reason for the lower occurrence rate is that the DE 1 search coil has been optimized for higher frequencies (up to 10 kHz) and is not as sensitive as the GEOS search coil at frequencies below 10 Hz, where ion cyclotron waves associated with heavy ions are most frequently observed.

An example of an intense electromagnetic ion cyclotron wave event detected by DE 1 is shown in Figure 28. The ion cyclotron waves in this case occur from 0505 to 0520 UT as

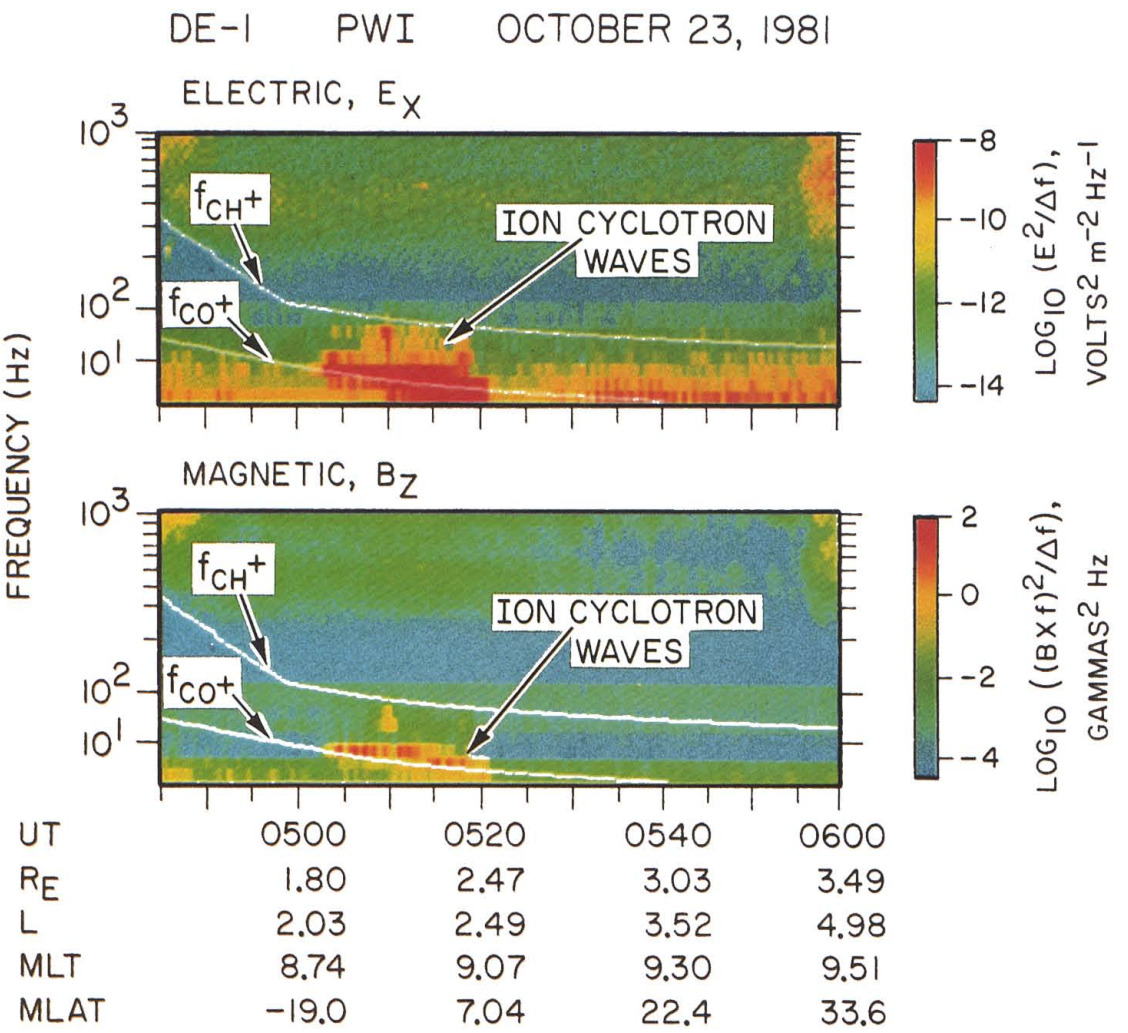

Fig. 28. An example of an electromagnetic ion cyclotron wave event detected by DE 1 deep inside the plasmasphere. This event is associated with strong heating of O^+ ions in the vicinity of the magnetic equator [*Quinn et al.*, 1986].

the spacecraft crosses the magnetic equator at a radial distance of about 2.2 R_E, deep inside the plasmasphere. The primary emission frequency is about 3–6 Hz, slightly above the O^+ ion cyclotron frequency. The energetic ion composition spectrometer on DE 1 showed that these waves are closely associated with a nonthermal (~ 10 eV to 2 keV) O^+ ion conic distribution [*Quinn et al.*, 1986]. Both the waves and the particles are confined to a relatively narrow range of magnetic latitudes, 13°–18°, centered on the magnetic equator. The close spatial relationship of the two phenomena strongly indicates that the ion cyclotron waves are responsible for accelerating the O^+ ions.

Other studies of the equatorial waves and their relationship to the local plasma population have been performed by *Olsen et al.* [1987] using the DE 1 data. Their studies demonstrated a close correspondence between plasma heating and the occurrence of electromagnetic ion Bernstein waves. An example of this relationship is shown in Figure 29, from *Olsen et al.* [1987]. The top two panels show proton energy and pitch angle spectrograms obtained from the retarding ion mass spectrometer during a south-to-north pass through the magnetic equator at about 5.5 R_E. During this pass a very intense, strongly heated proton distribution was encountered in a region centered on the magnetic equator. The latitudinal width of this region is only ±5°. The temperature and peak density of the protons is estimated to be 6.7 eV and 12 cm^{-3}. The pitch angle spectrogram shows that the protons are sharply peaked at a pitch angle of 90°. The bottom panel of Figure 29 shows the plasma wave electric field spectrogram. The electron and proton cyclotron frequencies are indicated by the white lines labeled f_{ce} and f_{ci}. The line labeled f_{LHR} is the lower hybrid resonance frequency, which has been computed by taking the geometric mean of the electron and ion cyclotron frequencies: $f_{LHR} \simeq (f_{ce} f_{ci})^{1/2}$. The bright red spot immediately below the lower hybrid resonance frequency and centered almost exactly on the magnetic equator is the electromagnetic ion Bernstein mode emissions. These emissions are most intense at frequencies in the range around a few hundred hertz, between f_{ci} and f_{LHR}. An enhancement can also be seen just above f_{ci}.

Although the harmonic structure cannot be seen in the low-resolution spectrogram shown in Figure 29, comparison with other examples, such as those published by *Gurnett* [1976], clearly identifies the noise between f_{ci} and f_{LHR} as electromagnetic ion Bernstein mode emissions. Several additional examples of these emissions have been identified and analyzed by *Olsen et al.* [1987]. In all cases the waves are found to be associated with strongly heated equatorial ion populations.

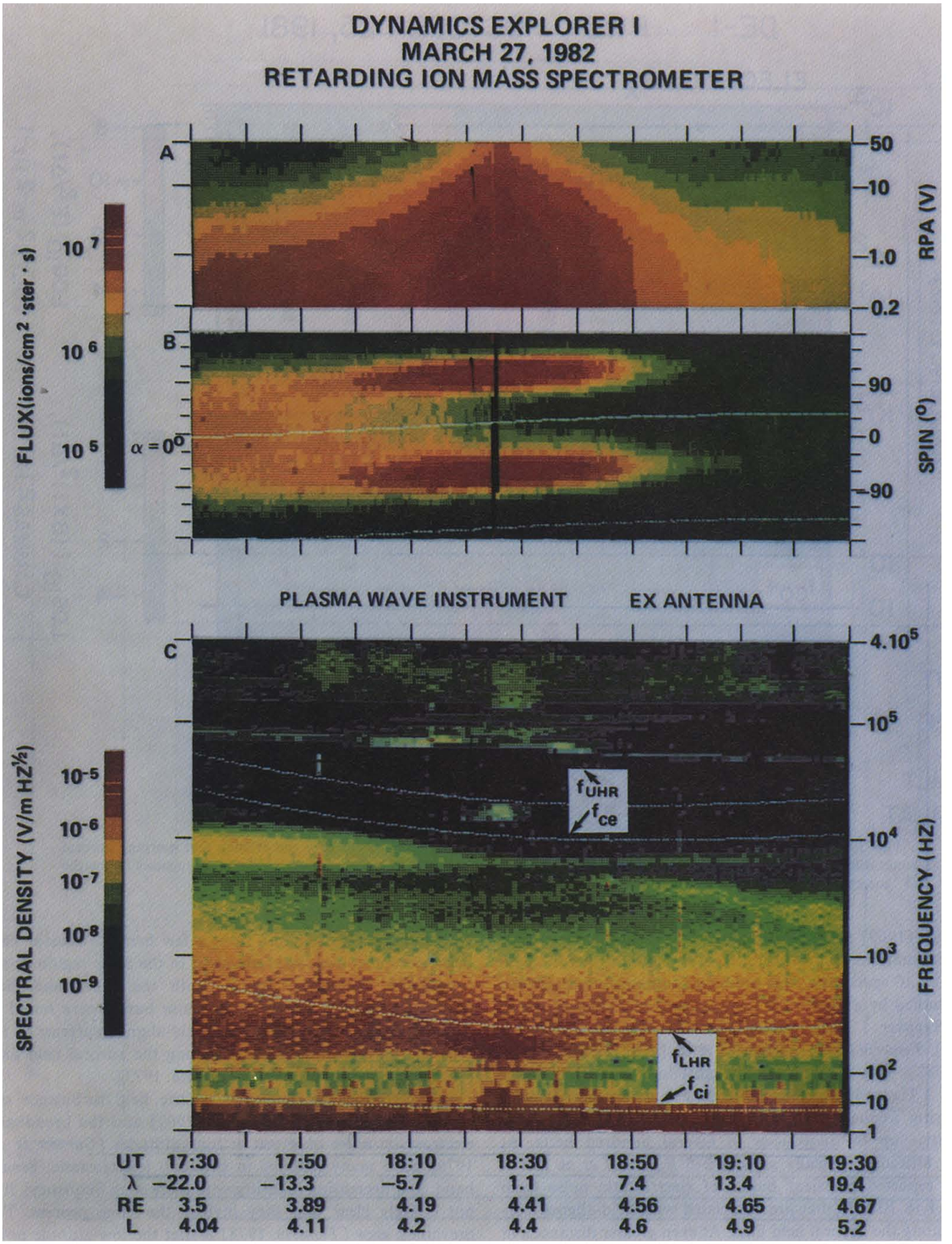

Fig. 29. An example of an electromagnetic ion Bernstein mode event detected by DE 1 in association with a region of strong H^+ ion heating near the magnetic equatorial plane. The ion Bernstein mode emissions occur slightly below the lower hybrid frequency f_{LHR}, from about 1820 to 1840 UT [from *Olsen et al.*, 1987].

These comparisons strongly suggest that the waves play an important role in ion heating. Specific mechanisms by which ion Bernstein mode waves can heat the ions are discussed by *Curtis* [1985].

8. Low-Frequency Waves and Turbulence Along the Auroral Field Lines

The existence of intense low-frequency electric field noise along the auroral field lines has been known for many years.

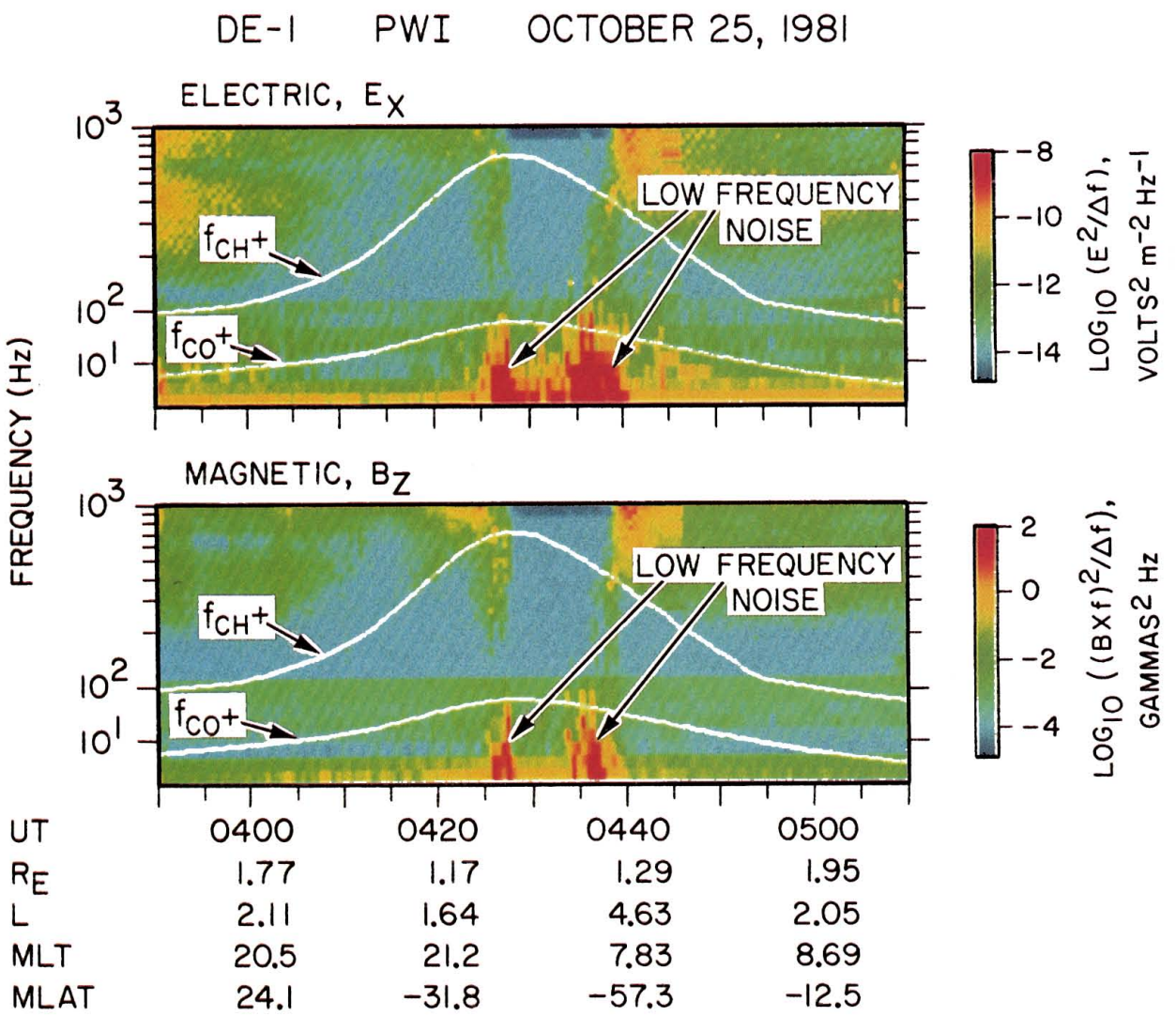

Fig. 30. An example of broadband electric and magnetic field noise observed over the evening and morning auroral zones during a low-altitude DE 1 pass over the southern polar region. The noise is most intense at frequencies below the O^+ ion cyclotron frequency [from *Gurnett et al.*, 1984].

Heppner [1969] first reported observations of intense electric field fluctuations at low altitudes over the auroral zone with the OV1-10 spacecraft. This noise was subsequently described and studied by a number of investigators, including *Maynard and Heppner* [1970], *Kelley and Mozer* [1972], *Kintner* [1976], *Temerin* [1978], *Maynard et al.* [1982], and *Curtis et al.* [1982]. This noise is usually most intense at frequencies below 1 Hz and decreases more or less monotonically with increasing frequency, sometimes extending with measurable intensities up to frequencies of several hundred hertz. At higher altitudes, typically around 2–5 R_E, *Scarf et al.* [1973, 1975] reported transient bursts of electrostatic noise from about 1 to 10 kHz that are associated with field-aligned currents along the auroral field lines. At even greater distances, in the distant magnetotail, *Gurnett et al.* [1976] reported observations of intense electrostatic noise extending over a broad range of frequencies, from typically a few hertz to a few kilohertz. This noise was called "broadband electrostatic noise." Subsequent studies by *Gurnett and Frank* [1977] showed that the broadband electrostatic noise extended along the auroral field lines from altitudes of a few thousand kilometers to many Earth radii in the distant magnetotail. Magnetic noise bursts with frequencies extending from a few hertz to several kilohertz were also frequently observed in the same region as the broadband electrostatic noise. Both the broadband electrostatic noise and the magnetic noise bursts were found to occur in regions with substantial field-aligned currents of the type that is frequently observed along the auroral field lines [*Armstrong and Zmuda*, 1973; *Fairfield*, 1973].

Although the low-frequency electric field turbulence observed at low altitudes [*Heppner*, 1969] and the broadband electrostatic noise observed at high altitudes [*Gurnett et al.*, 1976] have many features in common (electrostatic, broadband, and decreasing intensity with increasing frequency), it is not entirely clear that they involve the same process. The prevailing view [*Temerin*, 1978] is that the low-altitude noise consists of short-wavelength quasi-static turbulence that is Doppler-shifted upward in frequency by the spacecraft motion relative to the plasma. On the other hand, the broadband electrostatic noise in the distant magnetotail is currently interpreted as an ion beam instability [*Grabbe and Eastman*, 1984]. Because of the uncertainties we will use the term "broadband noise" as a descriptive term with no implication regarding the mechanism or mechanisms involved in generating the noise.

Since DE 1 crosses the auroral field lines over a wide range of radial distances, numerous possibilities exist for making advances in the understanding of the broadband noise. At the present time, two types of studies have been completed. The first, by *Gurnett et al.* [1984], used the step frequency correlator to study frequencies from a few hertz to several hundred hertz, and the second, by *Weimer et al.* [1985, 1986, 1987], used the dc electric field channel (see Figure 2) and the magnetometer to study frequencies of a few hertz and below. Typical electric and magnetic field spectrograms of the broadband noise observed during a low-altitude pass over evening and morning auroral zones are shown in Figure 30. The auroral zone crossings are easily identified in these spectrograms by the abrupt burst of low-frequency electric and magnetic field noise from 0426 to 0428 UT and from 0435 to 0440 UT. Broadband noise bursts of this type are a persistent feature of the auroral zone and are observed on essentially all of the low-altitude DE 1 auroral zone crossings. The electric and magnetic field spectral densities for a representative auroral zone crossing are shown in Figure 31. The spectral densities decrease more or less monotonically with increasing frequency and are easily detectable above the receiver background noise at all frequencies up to about 1 kHz. The magnetic spectrum

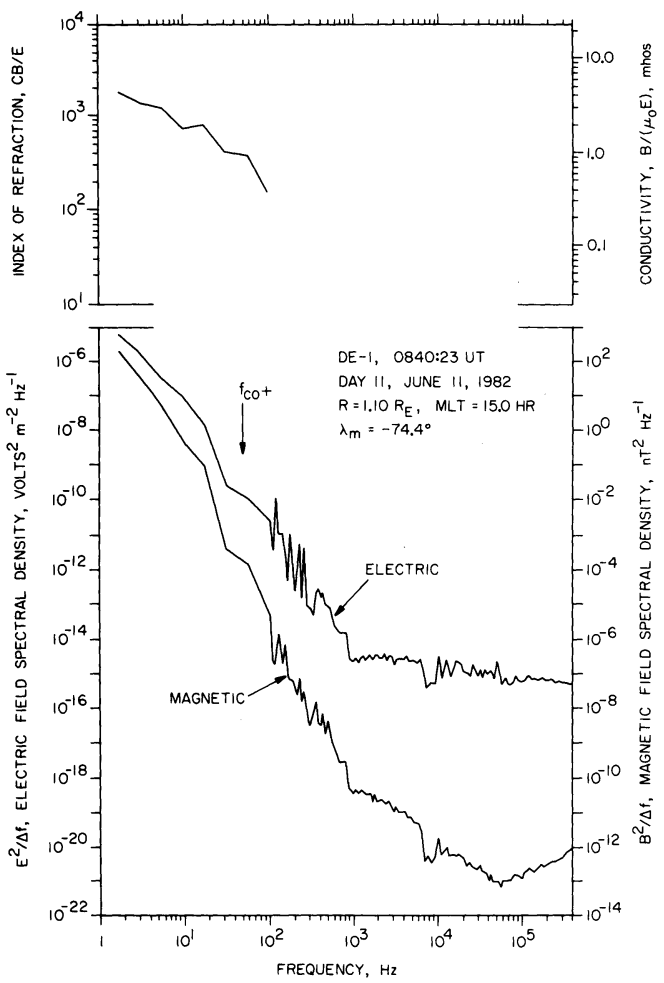

Fig. 31. Representative electric and magnetic spectrograms for a broadband auroral zone noise event comparable to those shown in Figure 30. The top panel shows the ratio of the magnetic to electric field strength in terms of the index of refraction for parallel propagation, cB/E, and in terms of the Pedersen conductivity $B/(\mu_0 E)$.

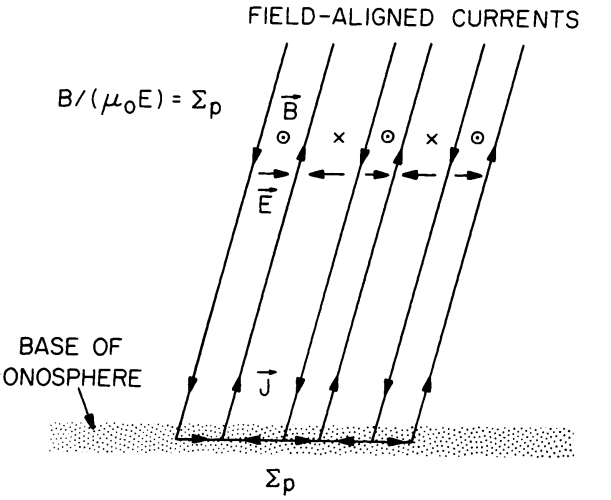

Fig. 32. An interpretation of the broadband low-frequency noise based on an assumed field-aligned current structure that closes through a conducting layer at the base of the ionosphere. A spacecraft crossing horizontally through this system would detect a spectrum of closely correlated electric and magnetic field fluctuations with $B/(\mu_0 E) = \Sigma_P$, the Pedersen conductivity.

is usually steeper than the electric field spectrum. Typical power law spectral indices are -3.0 to -5.0 for the magnetic field spectrum and -2.0 to -4.0 for the electric field spectrum. At low altitudes, below $\sim 2\ R_E$, both the electric and the magnetic field fluctuations are perpendicular to the static magnetic field. Correlator measurements [*Gurnett et al.*, 1984] show that the north-south electric field fluctuations are closely correlated with the east-west magnetic field fluctuations. The sign of the correlation is such that the Poynting flux (electromagnetic energy flow) is always directed downward, toward the Earth. Integrated over the entire auroral zone, the electromagnetic energy flow associated with these fluctuations is substantial, $\sim 10^8$ W.

Two basically different models have been advanced to explain this noise. The first model assumes that the noise is caused by the motion of the spacecraft through a system of static field-aligned current structures imbedded in the ionosphere, and the second assumes that the noise is caused by waves, most likely Alfvén waves. The essential feature of the static field model is shown in Figure 32. This model assumes that a system of field-aligned current sheets exists in the ionosphere that close through the base of the ionosphere via Pedersen currents. The field-aligned currents produce an east-west magnetic field **B** that is directly related to a north-south electric field **E**. The possible existence of such field structures in the ionosphere was first pointed out by *Smiddy et al.* [1980]. At high latitudes, where the geomagnetic field is nearly vertical, the magnetic to electric field ratio is given by the Pedersen conductivity, $B/(\mu_0 E) = \Sigma_P$. This proportionality explains the high correlation between the electric and magnetic field fluctuations. It is also easily verified that the Poynting flux is directed downward, toward the ionosphere, as is observed. The top panel of Figure 31 shows the measured $B/(\mu_0 E)$ ratio in units of conductivity. Although not constant, the observed $B/(\mu_0 E)$ ratios, from 2 to 10 mhos, are comparable to the Pedersen conductivities measured in auroral arcs by radar backscatter techniques [*Horowitz et al.*, 1978]. Although the observed $B/(\mu_0 E)$ ratios vary with frequency and are somewhat lower than would be expected from radar measurements, the dis-

agreements are not serious. At the highest frequencies, ~1 kHz, the spatial scale of the current structures is very small, ~10 m. At such small spatial lengths, some deviations from the Pedersen conductivity are to be expected.

The second mechanism for explaining the low-frequency electromagnetic noise assumes that the noise is caused by waves. At the very lowest frequencies, ~1 Hz, the waves would have to be Alfvén waves. In some cases the electric and magnetic field spectrums show a drop in intensity near the O^+ ion cyclotron frequency (see Figure 31). A decrease of this type is expected for an Alfvén wave, since the left-hand-polarized component (an electromagnetic ion cyclotron wave) cannot propagate at frequencies above the ion cyclotron frequency. Frequency components well above the ion cyclotron frequency (above about 10–100 Hz) cannot be attributed to Alfvén waves unless the wavelengths are short, tens of meters, so that large Doppler shifts are produced. A special type of Alfvén wave, called a kinetic Alfvén wave [*Hasegawa*, 1977], does exist which could have such short wavelengths, so this possibility cannot be entirely ruled out. If the waves are Alfvén waves, the cB/E ratio should be comparable to the Alfvén index of refraction. Typical Alfvén indices of refraction along the auroral field lines vary from about 10^3 at low altitudes in the ionosphere to about 10 at an altitude of 1 R_E. The left-hand scale in the top panel of Figure 31 shows that the measured cB/E ratios are approximately 10^3, which is in reasonable agreement with the expected Alfvén index of refraction at low altitudes. Other studies by *Gurnett et al.* [1984] show that the cB/E ratio decreases with increasing altitude, although not quite as rapidly as would be expected for the Alfvén index of refraction.

If the low-frequency electromagnetic noise is caused by Alfvén waves, this noise may play an important role in accelerating ions along the auroral field lines. In a specific example, *Chang et al.* [1986] have analyzed a case in which an O^+ ion conic distribution was observed in a region of intense low-frequency noise. Their analysis showed that the O^+ ion conic distribution could be explained if the electric field noise provides transverse stochastic acceleration of the ions as they spiral upward along the auroral field lines.

Studies of the broadband low-frequency noise have also been carried out by *Weimer et al.* [1985] using the dc electric field channel, which provides measurements up to 8 Hz. This study concentrated on magnetic conjunctions, when both DE 1 and DE 2 were nearly on the same magnetic field line as the spacecraft passed over the auroral zone. Although no comparisons were made with the higher-frequency measurements, it is virtually certain that the fluctuations detected in the dc channel represent the low-frequency extension of the broadband noise shown in Figure 31. In the analysis of *Weimer et al.* [1985] it was assumed that the fluctuations are caused by the motion of the spacecraft through static field-aligned structures. Comparisons of low-altitude electric field spectrums measured by DE 2 with high-altitude magnetic field spectrums measured by DE 1 showed very good agreement when mapped to a common wave number scale. An example of these comparisons is shown in Figure 33. The similarity in the spectrums at two widely located points along the same magnetic field line provides strong evidence that the fluctuations are caused by a field-aligned current system and not by waves. The $B/(\mu_0 E)$ ratio gives a Pedersen conductivity of 6 mhos, which is a very reasonable value. When the electric fields measured by DE 1 and DE 2 are compared using a similar mapping technique, the spectrums are in good agreement at low

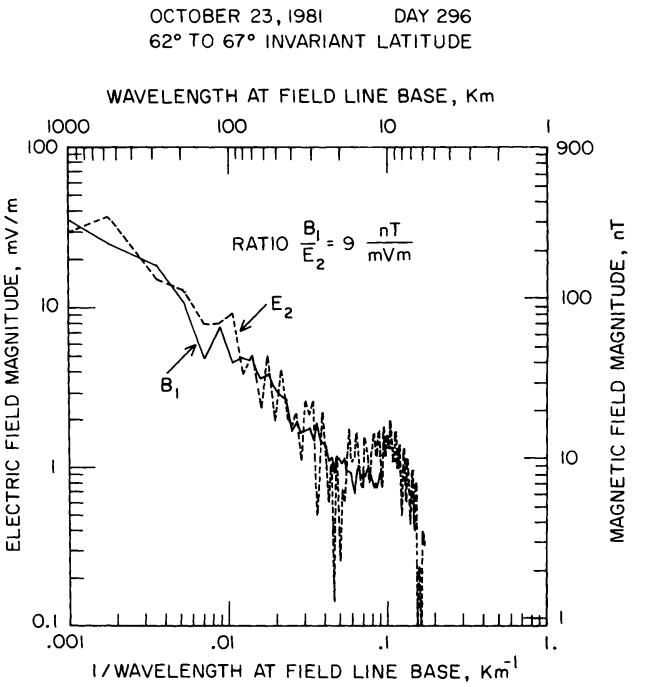

Fig. 33. A comparison of an electric field spectrum E_2 from DE 2 with a magnetic field spectrum B_1 from DE 1 during a magnetic conjunction over the evening auroral zone. The close similarity of the high-altitude magnetic field spectrum to the low-altitude electric field spectrum provides strong evidence that the noise is caused by a system of static field-aligned current structures linking the two spacecraft [from *Weimer et al.*, 1985].

frequencies (wavelengths greater than 100 km) but disagree at high frequencies. An example of these comparisons is shown in Figure 34. Typically, the high-frequency electric fields are more intense at high altitudes (DE 1) than at low altitudes (DE 2).

The magnetic conjunction studies with DE 1 and DE 2 show tht long-wavelength electric fields are mapped from high to low altitudes with little or no attenuation and that short-wavelength fields, less than 100 km, are strongly attenuated. These results have been interpreted by *Weimer et al.* [1985] in terms of an effective "Ohm's law" conductivity along the auroral field line, based on the theory of *Lyons* [1980]. Typical values estimated for the conductance are of the order of 10^{-8} mho/m^2. The existence of a conductance in the field-aligned current system indicates that large potential drops exist along the auroral field lines. Such potential drops are believed to play an important role in the acceleration of auroral electrons.

9. Conclusion

The results presented in this review illustrate the wide range of plasma wave phenomena that can be studied with the Dynamics Explorer 1 spacecraft. Although many important questions have been answered, there are still many areas of magnetospheric plasma wave research that can still be explored with the DE 1 data. This is especially true for correlative studies with other instruments and for multispacecraft studies. Such studies often required advanced data sets in which certain favorable geometries or geophysical conditions are present. For example, studies of field-aligned potential gradients require magnetic conjunctions, and comparisons

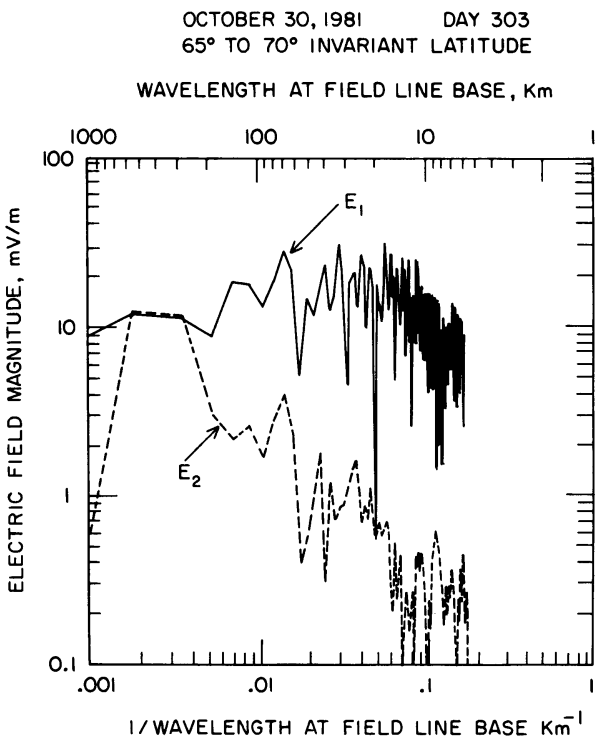

Fig. 34. A comparison of the electric field spectrums from DE 1 and DE 2 for a magnetic conjunction similar to that shown in Figure 33. The spectrums are in good quantitative agreement at low frequencies (wavelengths longer than about 100 km) but diverge strongly at higher frequencies, with higher intensities at DE 1. These observations show that short-wavelength fields are not mapped effectively from high to low altitudes.

with auroral phenomena require auroral images when certain specified auroral phenomena are present. Although a few such events have been identified and studied, much remains to be done. The DE plasma wave data still have great potential for correlative investigations with other instruments and spacecraft.

Acknowledgments. The authors would like to express their special thanks to R. Huff, who helped prepare several of the illustrations used in this review. The research at the University of Iowa was supported by NASA through grant NAS5-310 with Goddard Space Flight Center and by grant NGL 16-001-043 from NASA Headquarters. The research at Stanford University was supported by NASA through grant NAG5-476.

REFERENCES

Allcock, G. M., A study of the audio-frequency radio phenomenon known as "dawn chorus," *Aust. J. Phys., 10*, 286, 1957.

Armstrong, J. C., and A. J. Zmuda, Triaxial magnetic measurements of field-aligned currents at 800 km in the auroral region: Initial results, *J. Geophys. Res., 78*, 6802, 1973.

Barkhausen, H., Zwei mit Hilfe der neuen Verstärker entdeckte Erscheinungen, *Phys. Z., 20*, 401, 1919.

Bell, T. F., and H. D. Ngo, Electrostatic waves stimulated by coherent VLF signals propagating in and near the inner radiation belt, *J. Geophys. Res., 93*, 2599, 1988.

Bell, T. F., U. S. Inan, and R. A. Helliwell, Nonducted coherent VLF waves and associated triggered emissions observed on the ISEE 1 satellite, *J. Geophys. Res., 86*, 4649, 1981.

Bell, T. F., H. G. James, U. S. Inan, and J. P. Katsufrakis, The apparent spectral broadening of VLF transmitter signals during transionospheric propagation, *J. Geophys. Res., 88*, 4813, 1983.

Benson, R. F., Harmonic auroral kilometric radiation of natural origin, *Geophys. Res. Lett., 9*, 1120, 1982.

Benson, R. F., Ordinary mode auroral kilometric radiation with harmonics observed by ISIS 1, *Radio Sci., 19*, 543, 1984.

Benson, R. F., Auroral kilometric radiation: Wave modes, harmonics, and source region density structures, *J. Geophys. Res., 90*, 2753, 1985.

Benson, R. F., and W. Calvert, ISIS 1 observations at the source of auroral kilometric radiation, *Geophys. Res. Lett., 6*, 479, 1979.

Benson, R. F., M. M. Mellott, R. L. Huff, and D. A. Gurnett, Ordinary mode auroral kilometric radiation fine structure observed by DE 1, *J. Geophys. Res., 93*, 7515, 1988.

Budden, K. G., *Radio Waves in the Ionosphere*, Cambridge University Press, New York, 1961.

Burch, J. L., J. D. Winningham, V. A. Blevins, N. Eaker, W. C. Gibson, and R. A. Hoffman, High-altitude plasma instrument for Dynamics Explorer-A, *Space Sci. Instrum., 5*, 455, 1981.

Burch, J. L., P. H. Reiff, and M. Sugiura, Upward electron beams measured by DE-1: A primary source of dayside region 1 Birkeland currents, *Geophys. Res. Lett., 10*, 753, 1983.

Burtis, W. J., and R. A. Helliwell, Magnetospheric chorus: Occurrence patterns and normalized frequency, *Planet. Space Sci., 24*, 1007, 1976.

Calvert, W., The auroral plasma cavity, *Geophys. Res. Lett., 8*, 919, 1981.

Calvert, W., Harmonics and related ISIS-1 AKR observations (abstract), *Eos Trans. AGU, 64*, 815, 1983.

Calvert, W., DE 1 measurements of AKR wave directions, *Geophys. Res. Lett., 12*, 381, 1985.

Carpenter, D. L., and J. W. LaBelle, A study of whistlers correlated with bursts of electron precipitation near $L = 2$, *J. Geophys. Res., 87*, 4427, 1982.

Carpenter, D. L., F. Walter, R. E. Barrington, and D. J. McEwen, Alouette 1 and 2 observations of abrupt changes in whistler rate and of VLF noise variations at the plasmapause—A satellite-ground study, *J. Geophys. Res., 73*, 2929, 1968.

Chang, T., G. B. Crew, N. Hershkowitz, J. R. Jasperse, J. M. Retterer, and J. D. Winningham, Transverse acceleration of oxygen ions by electromagnetic ion cyclotron resonance with broadband left-hand polarized waves, *Geophys. Res. Lett., 13*, 636, 1986.

Chappell, C. R., S. A. Fields, C. R. Baugher, J. H. Hoffman, W. B. Hanson, W. W. Right, H. D. Hammack, G. R. Carignan, and A. F. Nagy, The retarding ion mass spectrometer on Dynamics Explorer-A, *Space Sci. Instrum., 5*, 477, 1981.

Cornwall, J. M., F. V. Coroniti, and R. M. Thorne, Turbulent loss of ring current protons, *J. Geophys. Res., 75*, 4699, 1970.

Curtis, S. A., Equatorial trapped plasmasphere ion distributions and transverse stochastic acceleration, *J. Geophys. Res., 90*, 1765, 1985.

Curtis, S. A., W. R. Hoegy, L. H. Brace, N. C. Maynard, and M. Sugiura, DE-2 cusp observations: Role of plasma instabilities in topside ionospheric heating and density fluctuations, *Geophys. Res. Lett., 9*, 997, 1982.

D'Angelo, N., and R. W. Motley, Electrostatic oscillations near the ion cyclotron frequency, *Phys. Fluids, 5*, 633, 1962.

Eckersley, T. L., 1929-1930 developments in the study of radio propagation, *Marconi Rev., 5*, 1, 1931.

Edgar, B. C., The upper and lower frequency cutoffs of magnetospherically reflected whistlers, *J. Geophys. Res., 81*, 205, 1976.

Ellis, G. R., Low-frequency radio emission from aurorae, *J. Atmos. Terr. Phys., 10*, 302, 1957.

Fairfield, D. H., Magnetic field signatures of substorms on high-latitude field lines in the magnetosphere, *J. Geophys. Res., 78*, 1553, 1973.

Farthing, W. H., M. Sugiura, B. G. Ledley, and L. J. Cahill, Jr., Magnetic field observations on DE-1 and -B, *Space Sci. Instrum., 5*, 551, 1981.

Frank, L. A., J. D. Craven, K. L. Ackerson, M. R. English, R. H. Eather, and R. L. Carovillano, Global auroral imaging instrumentation for the Dynamics Explorer Mission, *Space Sci. Instrum., 5*, 369, 1981.

Fredricks, R. W., Structure of generalized ion Bernstein modes from the full electromagnetic dispersion relation, *J. Plasma Phys., 2*, 365, 1968.

Fredricks, R. W., C. F. Kennel, F. L. Scarf, G. M. Crook, and I. M. Green, Detection of electric field turbulence in the Earth's bow shock, *Phys. Rev. Lett., 21*, 1761, 1968.

Gendrin, R., General relationships between wave amplification and particle diffusion in a magnetoplasma, *Rev. Geophys., 19*, 171, 1981.

Gendrin, R., and A. Roux, Energization of helium ions by proton-induced hydromagnetic waves, *J. Geophys. Res., 85*, 4577, 1980.

Goldberg, R. A., J. R. Barcus, L. C. Hale, and S. A. Curtis, Direct

observation of magnetospheric electron stimulation by lightning, *J. Atmos. Terr. Phys.*, *48*, 293, 1986.

Grabbe, C. L., and T. E. Eastman, Generation of broadband electrostatic noise by ion beam instabilities in the magnetotail, *J. Geophys. Res.*, *89*, 3865, 1984.

Gregory, P. C., Radio emission from auroral electrons, *Nature*, *221*, 350, 1969.

Gurnett, D. A., A satellite study of VLF hiss, *J. Geophys. Res.*, *71*, 5599, 1966.

Gurnett, D. A., The Earth as a radio source: Terrestrial kilometric radiation, *J. Geophys. Res.*, *79*, 4227, 1974.

Gurnett, D. A., The Earth as a radio source: The nonthermal continuum, *J. Geophys. Res.*, *80*, 2751, 1975.

Gurnett, D. A., Plasma wave interactions with energetic ions near the magnetic equator, *J. Geophys. Res.*, *81*, 2765, 1976.

Gurnett, D. A., and L. A. Frank, VLF hiss and related plasma observations in the polar magnetosphere, *J. Geophys. Res.*, *77*, 172, 1972.

Gurnett, D. A., and L. A. Frank, Continuum radiation associated with low-energy electrons in the outer radiation zone, *J. Geophys. Res.*, *81*, 3875, 1976.

Gurnett, D. A., and L. A. Frank, A region of intense plasma wave turbulence on auroral field lines, *J. Geophys. Res.*, *82*, 1031, 1977.

Gurnett, D. A., and J. L. Green, On the polarization and origin of auroral kilometric radiation, *J. Geophys. Res.*, *83*, 689, 1978.

Gurnett, D. A., and A. M. Persoon, Electron density measurements using the plasma frequency cutoff of auroral hiss, *Eos Trans. AGU*, *68*, 1434, 1987.

Gurnett, D. A., and R. R. Shaw, Electromagnetic radiation trapped in the magnetosphere above the plasma frequency, *J. Geophys. Res.*, *78*, 8136, 1973.

Gurnett, D. A., L. A. Frank, and R. P. Lepping, Plasma waves in the distant magnetotail, *J. Geophys. Res.*, *81*, 6059, 1976.

Gurnett, D. A., R. R. Anderson, F. L. Scarf, R. W. Fredricks, and E. J. Smith, Initial results from the ISEE-1 and -2 plasma wave investigation, *Space Sci. Rev.*, *23*, 103, 1979.

Gurnett, D. A., S. D. Shawhan, and R. R. Shaw, Auroral hiss, *Z* mode radiation, and auroral kilometric radiation in the polar magnetosphere: DE 1 observations, *J. Geophys. Res.*, *88*, 329, 1983.

Gurnett, D. A., R. L. Huff, J. D. Menietti, J. L. Burch, J. D. Winningham, and S. D. Shawhan, Correlated low-frequency electric and magnetic noise along the auroral field lines, *J. Geophys. Res.*, *89*, 8971, 1984.

Gurnett, D. A., W. Calvert, R. L. Huff, D. Jones, and M. Sugiura, The polarization of escaping terrestrial continuum radiation, *J. Geophys. Res.*, in press, 1988.

Harris, E. G., Unstable plasma oscillations in a magnetic field, *Phys. Rev. Lett.*, *2*, 34, 1959.

Hartz, T. R., Radio noise levels within and above the ionosphere, *Proc. IEEE*, *57*, 1024, 1969.

Hasegawa, A., Kinetic properties of Alfvén waves, *Proc. Indian Acad. Sci.*, *86*, 151, 1977.

Hashimoto, K., W. Calvert, and R. Huff, On *Z*-mode waves observed by the DE-1 satellite, paper presented at Solar Terrestrial Environment Workshop, Soc. of Geomagn. and Earth, Planet. and Space Sci., Tokyo, Jan. 22, 1987.

Helliwell, R. A., *Whistlers and Related Ionospheric Phenomena*, Stanford University Press, Stanford, Calif., 1965.

Helliwell, R. A., J. P. Katsufrakis, and M. L. Trimpi, Whistler-induced amplitude perturbation in VLF propagation, *J. Geophys. Res.*, *78*, 4679, 1973.

Helliwell, R. A., S. B. Mende, J. H. Doolittle, W. C. Armstrong, and D. L. Carpenter, Correlations between λ4278 optical emissions and VLF wave events observed at $L \simeq 4$ in the Antarctic, *J. Geophys. Res.*, *85*, 3376, 1980.

Heppner, J. P., Magnetospheric convection patterns inferred from high latitude activity, in *Atmospheric Emissions*, edited by B. M. McCormac and A. Omholt, p. 251, Reinhold, New York, 1969.

Hoffman, R. A., and E. R. Schmerling, Dynamics Explorer Program: An overview, *Space Sci. Instrum.*, *5*, 345, 1981.

Horita, R. E., and H. G. James, Source regions deduced from attenuation bands in VLF saucers, *J. Geophys. Res.*, *87*, 9147, 1982.

Horowitz, J. L., J. R. Doupnik, and P. M. Banks, Chatanika radar observations of the latitudinal distributions of auroral zone electric fields, conductivities, and currents, *J. Geophys. Res.*, *83*, 1463, 1978.

Huff, R. L., W. Calvert, J. D. Craven, L. A. Frank, and D. A. Gurnett, Mapping of auroral kilometric radiation sources to the aurora, *J. Geophys. Res.*, in press, 1988.

Imhof, W. L., J. B. Reagan, H. D. Voss, E. E. Gaines, D. W. Datlowe, J. Mobilia, R. A. Helliwell, U. S. Inan, J. P. Katsufrakis, and R. G. Joiner, Direct observation of radiation belt electrons precipitated by controlled injection of VLF signals from a ground-based transmitter, *Geophys. Res. Lett.*, *10*, 361, 1983*a*.

Imhof, W. L., J. B. Reagan, H. D. Voss, E. E. Gaines, D. W. Datlowe, J. Mobilia, R. A. Helliwell, U. S. Inan, J. P. Katsufrakis, and R. G. Joiner, The modulated precipitation of radiation belt electrons by controlled signals from VLF transmitters, *Geophys. Res. Lett.*, *10*, 615, 1983*b*.

Imhof, W. L., J. B. Reagan, E. E. Gaines, and D. W. Datlowe, The *L* shell region of importance for waves emitted at ground level as a loss mechanism for trapped electrons >68 keV, *J. Geophys. Res.*, *89*, 827, 1984.

Imhof, W. L., H. D. Voss, M. Walt, E. E. Gaines, J. Mobilia, D. W. Datlowe, and J. B. Reagan, Slot region electron precipitation by lightning, VLF chorus, and plasmaspheric hiss, report, Lockheed Palo Alto Res. Lab., Palo Alto, Calif., March 31, 1986.

Inan, U. S., and T. F. Bell, Spectral broadening of VLF transmitter signals observed on DE-1: A quasi-electrostatic phenomenon?, *J. Geophys. Res.*, *90*, 1771, 1985.

Inan, U. S., and D. L. Carpenter, On the correlation of whistlers and associated subionospheric VLF/LF perturbations, *J. Geophys. Res.*, *91*, 3106, 1986.

Inan, U. S., and D. L. Carpenter, Lightning-induced electron precipitation events observed at $L \sim 2.4$ as phase and amplitude perturbations on subionospheric VLF signals, *J. Geophys. Res.*, *92*, 3293, 1987.

Inan, U. S., D. L. Carpenter, R. A. Helliwell, and J. P. Katsufrakis, Subionospheric VLF/LF phase perturbations produced by lightning-whistler induced particle precipitation, *J. Geophys. Res.*, *90*, 7457, 1985.

James, H. G., VLF saucers, *J. Geophys. Res.*, *81*, 501, 1976.

Jones, D., Source of terrestrial non-thermal radiation, *Nature*, *260*, 686, 1976.

Jones, D., Latitudinal beaming of planetary radio emissions, *Nature*, *288*, 225, 1980.

Jones, D., Terrestrial myriametric radiation from the Earth's plasmapause, *Planet. Space Sci.*, *30*, 399, 1982.

Jones, D., W. Calvert, D. A. Gurnett, and R. L. Huff, Observed beaming of terrestrial myriametric radiation, *Nature*, *328*, 391, 1987.

Jorgensen, T. S., Interpretation of auroral hiss measured on OGO 2 and at Byrd Station in terms of incoherent Cerenkov radiation, *J. Geophys. Res.*, *73*, 1055, 1968.

Kaiser, M. L., J. K. Alexander, A. C. Riddle, J. B. Pearce, and J. W. Warwick, Direct measurements by Voyager 1 and 2 of the polarization of terrestrial kilometric radiation, *Geophys. Res. Lett.*, *5*, 857, 1978.

Kelley, M. C., and F. S. Mozer, A satellite survey of vector electric fields in the ionosphere at frequencies of 10 to 500 Hz, 1, Isotropic, high-latitude electrostatic emissions, *J. Geophys. Res.*, *77*, 4158, 1972.

Kennel, C. F., and H. E. Petschek, Limit on stably trapped particle fluxes, *J. Geophys. Res.*, *71*, 1, 1966.

Kennel, C. F., F. L. Scarf, R. W. Fredricks, J. H. McGehee, and F. V. Coroniti, VLF electric field observations in the magnetosphere, *J. Geophys. Res.*, *75*, 6136, 1970.

Kindel, J. M., and C. F. Kennel, Topside current instabilities, *J. Geophys. Res.*, *76*, 3055, 1971.

Kintner, P. M., Jr., Observations of velocity shear driven plasma turbulence, *J. Geophys. Res.*, *81*, 5114, 1976.

Kintner, P. M., Jr., and D. A. Gurnett, Observations of ion cyclotron waves within the plasmasphere, *J. Geophys. Res.*, *82*, 2314, 1977.

Kovrazhkin, R. A., M. M. Mogilevsky, O. A. Moltchanov, Yu. I. Galperin, N. V. Djordjio, Yu. V. Lissakov, J. M. Bosqued, and H. Reme, Direct detection of the precipitation of ring current electrons and protons stimulated by artificial VLF emission, *Geophys. Res. Lett.*, *11*, 705, 1984.

Krall, N. A., and A. W. Trivelpiece, *Principles of Plasma Physics*, McGraw-Hill, New York, 1973.

Kurth, W. S., J. D. Craven, L. A. Frank, and D. A. Gurnett, Intense electrostatic waves near the upper hybrid resonance frequency, *J. Geophys. Res.*, *84*, 4145, 1979.

Kurth, W. S., D. A. Gurnett, and R. R. Anderson, Escaping nonthermal continuum radiation, *J. Geophys. Res.*, *86*, 5519, 1981.

Laaspere, T., and R. A. Hoffman, New results on the correlation

between low-energy electrons and auroral hiss, *J. Geophys. Res.*, *81*, 524, 1976.

Lee, L. C., J. R. Kan, and C. S. Wu, Generation of AKR and the structure of auroral acceleration region, *Planet. Space Sci.*, *28*, 703, 1980.

Lin, C. S., J. L. Burch, S. D. Shawhan, and D. A. Gurnett, Correlation of auroral hiss and upward electron beams near the polar cusp, *J. Geophys. Res.*, *89*, 925, 1984.

Lyons, L. R., Generation of large-scale regions of auroral currents, electric potentials, and precipitation by divergence at the convection electric fields, *J. Geophys. Res.*, *85*, 17, 1980.

Lyons, L. R., and D. J. Williams, *Quantitative Aspects of Magnetosphere Physics*, D. Reidel, Hingham, Mass., 1984.

Maggs, J. E., Coherent generation of VLF hiss, *J. Geophys. Res.*, *81*, 1707, 1976.

Mauk, B. H., C. E. McIlwain, and R. L. McPherron, Helium cyclotron resonance within the Earth's magnetosphere, *Geophys. Res. Lett.*, *8*, 103, 1981.

Maynard, N. C., and J. P. Heppner, Variations in electric fields from polar orbiting satellites, in *Particles and Fields in the Magnetosphere*, edited by B. M McCormac, p. 247, Reinhold, New York, 1970.

Maynard, N. C., J. P. Heppner, and A. Egeland, Intense, variable electric fields at ionospheric altitudes in the high latitude regions as observed by DE-2, *Geophys. Res. Lett.*, *9*, 981, 1982.

Mellott, M. M., W. Calvert, R. L. Huff, D. A. Gurnett, and S. D. Shawhan, DE-1 observations of ordinary mode and extraordinary mode auroral kilometric radiation, *Geophys. Res. Lett.*, *11*, 1188, 1984.

Mellott, M. M., R. L. Huff, and D. A. Gurnett, DE-1 observations of harmonic auroral kilometric radiation, *J. Geophys. Res.*, *91*, 13,732, 1986.

Melrose, D. B., Coherent gyromagnetic emission as a radiation mechanism, *Aust. J. Phys.*, *26*, 229, 1973.

Melrose, D. B., An interpretation of Jupiter's decametric radiation and the terrestrial kilometric radiation as direct amplified gyroemission, *Astrophys. J.*, *207*, 651, 1976.

Melrose, D. B., A theory for the nonthermal radio continuum in the terrestrial and Jovian magnetospheres, *J. Geophys. Res.*, *86*, 30, 1981.

Melrose, D. B., R. G. Hewitt, and G. A. Dulk, Electron-cyclotron maser emission: Relative growth and damping rates for different modes and harmonics, *J. Geophys. Res.*, *89*, 897, 1984.

Mosier, S. R., and D. A. Gurnett, VLF measurements of the Poynting flux along the geomagnetic field with the Injun 5 satellite, *J. Geophys. Res.*, *74*, 5675, 1969.

Muldrew, D. B., Preliminary results of ISIS 1 concerning electron density variations, ionospheric resonances and Cerenkov radiation, *Space Res.*, *10*, 786, 1970.

Olsen, R. C., Equatorially trapped plasma populations, *J. Geophys. Res.*, *86*, 11,235, 1981.

Olsen, R. C., S. D. Shawhan, D. L. Gallagher, J. L. Green, C. R. Chappell, and R. R. Anderson, Plasma observations at the Earth's magnetic equator, *J. Geophys. Res.*, *92*, 2385, 1987.

Oya, H., Origin of Jovian decameter wave emissions-conversion from the electron cyclotron plasma wave to the ordinary-mode electromagnetic wave, *Planet. Space Sci.*, *22*, 687, 1974.

Palmadesso, P., T. P. Coffey, S. L. Ossakow, and K. Papadopoulos, Generation of terrestrial kilometric radiation by a beam-driven electromagnetic instability, *J. Geophys. Res.*, *81*, 1762, 1976.

Persoon, A. M., D. A. Gurnett, and S. D. Shawhan, Polar cap electron densities from DE 1 plasma wave observations, *J. Geophys. Res.*, *88*, 10,123, 1983.

Persoon, A. M., D. A. Gurnett, W. K. Peterson, J. H. Waite, Jr., J. L. Burch, and J. L. Green, Electron density depletions in the nightside auroral zone, *J. Geophys. Res.*, *93*, 1871, 1988.

Poeverlein, H., Strahwege von Radiowellen in der Ionosphäre, *Z. Angew. Phys.*, *1*, 517, 1949.

Poulsen, W. L., and U. S. Inan, Satellite observations of a new type of discrete VLF emission at $L < 4$, *J. Geophys. Res.*, *93*, 1817, 1988.

~~Preece, W. H., Earth currents, *Nature*, *49*, 554, 1894.~~

Quinn, J. M., E. G. Shelley, H. L. Collin, and D. A. Gurnett, The generation of an O^+ conic distribution by equatorially confined waves as observed by DE-1, *Eos Trans. AGU*, *67*, 1138, 1986.

Rastani, K., U. S. Inan, and R. A. Helliwell, DE 1 observations of Siple transmitter signals and associated sidebands, *J. Geophys. Res.*, *90*, 4128, 1985.

Ratcliffe, J. A., *The Magneto-Ionic Theory and Its Applications to the Ionosphere*, Cambridge University Press, New York, 1959.

Rönnmark, K., H. Borg, P. J. Christiansen, M. P. Gough, and D. Jones, Banded electron cyclotron harmonic instability—A first comparison of theory and experiment, *Space Sci. Rev.*, *22*, 401, 1978.

Rosenberg, T. J., R. A. Helliwell, and J. P. Katsufrakis, Electron precipitation associated with discrete very low frequency emissions, *J. Geophys. Res.*, *76*, 8445, 1971.

Roux, A., and R. Pellat, Coherent generation of the auroral kilometric radiation by nonlinear beatings between electrostatic waves, *J. Geophys. Res.*, *84*, 5189, 1979.

Roux, A., S. Perrout, J. L. Rauch, C. deVilledary, G. Kremser, A. Knorth, and D. T. Young, Wave particle interactions near Ω_{He}^+ onboard GEOS 1 and 2: Generation of ion cyclotron waves and heating of He^+ ions, *J. Geophys. Res.*, *87*, 8174, 1982.

Russell, C. T., R. E. Holzer, and E. J. Smith, OGO 3 observations of ELF noise in the magnetosphere, 2, The nature of the equatorial noise, *J. Geophys. Res.*, *75*, 755, 1970.

Scarf, F. L., R. W. Fredricks, L. A. Frank, C. T. Russell, P. J. Coleman, Jr., and M. Neugebauer, Direct correlations of large-amplitude waves with suprathermal protons in the upstream solar wind, *J. Geophys. Res.*, *75*, 7316, 1970.

Scarf, F. L., R. W. Fredricks, L. A. Frank, and M. Neugebauer, Nonthermal electrons and high-frequency waves in the upstream solar wind, 1, Observations, *J. Geophys. Res.*, *76*, 5162, 1971.

Scarf, F. L., R. W. Fredricks, C. T. Russell, M. Kivelson, M. Neugebauer, and C. R. Chappell, Observation of a current-driven plasma instability at the outer zone–plasma sheet boundary, *J. Geophys. Res.*, *78*, 2150, 1973.

Scarf, F. L., R. W. Fredricks, C. T. Russell, M. Neugebauer, M. Kivelson, and C. R. Chappell, Current-driven plasma instabilities at high latitudes, *J. Geophys. Res.*, *80*, 2030, 1975.

Shawhan, S. D., Magnetospheric plasma waves, in *Solar System Plasma Physics*, vol. III, edited by L. J. Lanzerotti, C. F. Kennel, and E. N. Parker, p. 211, North-Holland, Amsterdam, 1979.

Shawhan, S. D., and D. A. Gurnett, Polarization measurements of auroral kilometric radiation by Dynamics Explorer-1, *Geophys. Res. Lett.*, *9*, 913, 1982.

Shawhan, S. D., D. A. Gurnett, D. L. Odem, R. A. Helliwell, and C. G. Park, The plasma wave and quasi-static electric field instrument (PWI) for Dynamics Explorer-A, *Space Sci. Instrum.*, *5*, 535, 1981.

Shelley, E. G., D. A. Simpson, T. C. Sanders, E. Hertzberg, H. Balsiger, and G. Ghielmetti, The energetic ion composition spectrometer (EICS) for the Dynamics Explorer-A, *Space Sci. Instrum.*, *5*, 443, 1981.

Smiddy, M., W. J. Burke, M. C. Kelley, N. A. Saflekos, M. S. Gussenhoven, D. A. Hardy, and F. J. Rich, Effects of high-altitude conductivity on observed convection electric fields and Birkeland currents, *J. Geophys. Res.*, *85*, 6811, 1980.

Smith, A. J., D. L. Carpenter, and U. S. Inan, Whistler-triggered VLF noise bursts observed on the DE-1 satellite and simultaneously at Antarctic ground stations, *Ann. Geophys.*, *3*(1), 81, 1985.

Smith, R. L., VLF observations of auroral beams as sources of a class of emissions, *Nature*, *224*, 351, 1969.

Sonwalkar, V. S., and U. S. Inan, Measurements of Siple transmitter signals on the DE 1 satellite: Wave normal direction and antenna effective length, *J. Geophys. Res.*, *91*, 154, 1986.

Sonwalker, V. S., and U. S. Inan, Wave normal direction and spectral properties of whistler mode hiss observed on the DE 1 satellite, *J. Geophys. Res.*, *93*, 7493, 1988.

Stix, T. H., *The Theory of Plasma Waves*, McGraw-Hill, New York, 1962.

Storey, L. R. O., An investigation of whistling atmospherics, *Philos. Trans. R. Soc. London, Ser. A.*, *246*, 113, 1953.

Tanaka, M., M. Hayakawa, D. Lagoutte, and F. Lefeuvre, Study of the middle latitude broadening of the spectrum of the waves emitted from ground, in *Results of the ARCAD 3 Project and of the Recent Programmes in Magnetospheric and Ionospheric Physics*, Cepadues-Editions, Toulouse, France, 1985.

Taylor, W. W. L., and L. R. Lyons, Simultaneous equatorial observations of 1- to 30-Hz waves and pitch angle distributions of ring current ions, *J. Geophys. Res.*, *81*, 6177, 1976.

Taylor, W. W. L., B. K. Parady, and L. J. Cahill, Jr., Explorer 45

Preece, W. H., Earth currents,
Nature, 49, 554, 1894.

observations of 1- to 30-Hz magnetic fields during magnetic storms, *J. Geophys. Res.*, *80*, 1271, 1975.

Temerin, M., The polarization, frequency, and wavelength of high-latitude turbulence, *J. Geophys. Res.*, *83*, 2609, 1978.

Titova, E. E., V. I. Di, V. E. Yurov, O. M. Raspapov, V. Yu. Trakhtengertz, F. Jiricek, and P. Triska, Interaction between VLF waves and the turbulent ionosphere, *Geophys. Res. Lett.*, *11*, 323, 1984.

Van Allen, J. A., G. H. Ludwig, E. C. Ray, and C. E. McIlwain, Observations of high intensity radiation by satellites 1958 alpha and gamma, *Rep. 28*, pp. 588–592, Jet Propulsion Lab., Pasadena, Calif., Sept. 1958.

Voss, H. D., W. L. Imhof, J. Mobilia, E. E. Gaines, M. Walt, U. S. Inan, R. A. Helliwell, D. L. Carpenter, J. P. Katsufrakis, and H. C. Chang, Lightning-induced electron precipitation, *Nature*, *312*, 740, 1984.

Weimer, D. R., C. K. Goertz, D. A. Gurnett, N. C. Maynard, J. L. Burch, Auroral zone electric fields from DE 1 and 2 at magnetic conjunctions, *J. Geophys. Res.*, *90*, 7479, 1985.

Weimer, D. R., D. A. Gurnett, and C. K. Goertz, The conductance of the auroral magnetic field lines, in *Ion Acceleration in the Magnetosphere and Ionosphere*, *Geophys. Monogr. Ser.*, vol. 38, edited by T. Chang, p. 108, AGU, Washington, D.C., 1986.

Weimer, D. R., D. A. Gurnett, C. K. Goertz, J. D. Menietti, J. L. Burch, and M. Sugiura, The current-voltage relationship in auroral current sheets, *J. Geophys. Res.*, *92*, 187, 1987.

Williams, D. J., Ring current composition and sources, in *Dynamics of the Magnetosphere*, edited by S.-I. Akasofu, p. 407, D. Reidel, Hingham, Mass., 1980.

Wu, C. S., and L. C. Lee, A theory of terrestrial kilometric radiation, *Astrophys. J.*, *230*, 621, 1979.

Wu, C. S., and X. M. Qiu, Emissions of second-harmonic auroral kilometric radiation, *J. Geophys. Res.*, *88*, 10,072, 1983.

D. A. Gurnett, Department of Physics and Astronomy, University of Iowa, Iowa City, IA 52242.

U. S. Inan, STAR Laboratory, Stanford University, Stanford, CA 94305.

(Received October 1, 1987;
accepted February 10, 1988.)